The Astrophysical Journal, 659:599–615, 2007 April 10

SPITZER IRAC AND JHK_S OBSERVATIONS OF h AND χ PERSEI: CONSTRAINTS ON PROTOPLANETARY DISK AND MASSIVE CLUSTER EVOLUTION AT $\sim 10^7$ YEARS

Thayne Currie,[1] Zoltan Balog,[2,3] S. J. Kenyon,[1] G. Rieke,[2] L. Prato,[4] E. T. Young,[2] J. Muzerolle,[2] D. P. Clemens,[5] M. Buie,[4] D. Sarcia,[5] A. Grabu,[5] E. V. Tollestrup,[5] B. Taylor,[4] E. Dunham,[4] and G. Mace[4]

Received 2006 September 18; accepted 2006 December 14

ABSTRACT

We describe IRAC 3.6–8 μm observations and ground-based near-IR JHK_s photometry from Mimir and 2MASS of the massive double cluster h and χ Persei complete to $J = 15.5$ ($M \sim 1.3\ M_\odot$). Within 25′ of the cluster centers we detect ~11,000 sources with $J \leq 15.5$, ~7000 sources with $[4.5] \leq 15$, and ~5000 sources with $[8] \leq 14.5$. In both clusters the surface density profiles derived from the 2MASS data decline with distance from the cluster centers as expected for a bound cluster. Within 15′ of the cluster centers, ~50% of the stars lie on a reddened ~13 Myr isochrone; at 15′–25′ from the cluster centers, ~40% lie on this isochrone. Thus, the optical/2MASS color-magnitude diagrams indicate that h and χ Per are accompanied by a halo population with roughly the same age and distance as the two dense clusters. The double cluster lacks any clear IR excess sources for $J \leq 13.5$ (~2.7 $M_\odot$). Therefore, disks around high-mass stars disperse prior to $\sim 10^7$ yr. At least 2%–3% of the fainter cluster stars have strong IR excess at both [5.8] and [8]. About 4%–8% of sources slightly more massive than the Sun (~1.4 $M_\odot$) have IR excesses at [8]. Combined with the lack of detectable excesses for brighter stars, this result suggests that disks around lower mass stars have longer lifetimes. The IR excess population also appears to be larger at longer IRAC bands ([5.8], [8]) than at shorter IRAC/2MASS bands (K_s, [4.5]), a result consistent with an inside-out clearing of disks.

Subject headings: circumstellar matter — infrared: stars — open clusters and associations: individual (NGC 869, NGC 884)

On-line material: color figures, machine-readable table

1. INTRODUCTION

The evolution of circumstellar disks sets strong constraints on the initial conditions for terrestrial and gas giant planet formation. In young stars the presence of circumstellar disks is inferred by near-to-mid infrared (IR) emission by dust in excess of the output of stellar photospheres. While the vast majority of stars in ~1 Myr clusters have disks, the frequency of disks declines on ~1–10 Myr timescales (e.g., Hillenbrand 2005; Young et al. 2004; Mamajek et al. 2004; Haisch et al. 2001). Because circumstellar dust is the evolutionary precursor to $\gtrsim 1$ km sized planetesimals, the timescale for the disappearance of dust emission, the "disk evolution timescale," is an important constraint for planet formation models (e.g., Strom et al. 1989; Hillenbrand 2005; Alibert et al. 2005; Currie 2005).

Recent observations of young ($\lesssim 10$ Myr) stars suggest that the evolution timescale may depend on stellar properties and locations within the disk. K band (~2 μm) excess from the inner ($r \lesssim 0.1$ AU) disk is relatively uncommon around both massive and very low mass stars (Hillenbrand et al. 1998). The ~5 Myr Upper Sco OB association also exhibits a mass-dependent frequency of disks: sources with IR excess at 8 μm and at 16 μm appear to be more prevalent around K/M and B/A stars than for F and G stars (Carpenter et al. 2006). Spatially resolved, mid-IR observations of ~3–5 Myr T Tauri stars (McCabe et al. 2006) show that many disks with strong mid-IR emission lack near-IR emission, providing evidence for a location-dependent disk evolution. The drop in near-IR circumstellar dust emission may be explained by grain growth, which is probably faster in the inner disk regions due to higher midplane densities and orbital frequencies (e.g., Dullemond & Dominik 2005). Circumstellar gas dispersal by UV photoevaporation (Clarke et al. 2001; Alexander et al. 2006) and planetesimal formation by gravitational instability (Youdin & Shu 2002; Youdin & Chiang 2004; Currie 2005) may also result in a location-dependent evolution and thus a wavelength-dependent timescale for the disappearance of near-IR emission.

Multiwavelength near-to-mid IR observations of evolved ($\gtrsim 10$ Myr), massive ($\gtrsim 1000$ members) clusters are required to measure the disk evolution timescale as a function of stellar mass and disk properties. The double cluster h and χ Per, the most massive, evolved open cluster within 3 kpc, provides a rich laboratory to study disk evolution in more detail. Starting with the initial study of Oosterhoff (1937), there has been much debate concerning the age, distance, and stellar content of the clusters (e.g., Borgman & Blaauw 1964; Wildey 1964; Schild 1967; Crawford et al. 1970; Vogt 1971; Tapia et al. 1984; Marco & Bernabeu 2001; Capilla & Fabregat 2002). Recent work (Keller et al. 2001; Slesnick et al. 2002, hereafter S02; Bragg & Kenyon 2005, hereafter BK05) has converged on a nearly identical age for both clusters, ~12–13 Myr, a common distance of ~2.34 kpc (a distance modulus ~11.85), a low extinction of $E(B - V) \sim 0.5$ uniform across the clusters (BK05), and an initial mass function (IMF) of massive stars consistent with results for other young, massive clusters (Massey 2003; Bragg 2004). Although the clusters have similar masses of $\gtrsim 4000\ M_\odot$ (h Per) and $\gtrsim 3000\ M_\odot$ (χ Per), the internal dynamical structure of the clusters may be very different (BK05), with some evidence for mass segregation in both clusters (S02, BK05).

[1] Harvard-Smithsonian Center for Astrophysics, Cambridge, MA 02140.
[2] Steward Observatory, University of Arizona, Tucson, AZ 85721.
[3] On leave from Department of Optics and Quantum Electronics, University of Szeged, H-6720, Szeged, Hungary.
[4] Lowell Observatory.
[5] Institute for Astrophysical Research, Boston University, Boston, MA 02215.

While numerous optical photometric and spectroscopic studies of h and χ Per exist, the cluster has yet to be explored in detail in the near-to-mid IR. Previous IR observations have been shallow, $J \sim K \lesssim 11-13$ (Tapia et al. 1984; Bragg & Kenyon 2002, respectively), and concentrated on understanding the population of Be stars. While some constraints have been placed on the stellar population of h and χ Per, the population of *circumstellar disks* remains unprobed. Thus, its potential to inform disk evolution theories remains untapped.

In this paper we describe the analysis of the first deep IR survey of h and χ Per. The survey combines 2MASS All-Sky Survey (2MASS) and Infrared Array Camera (IRAC, on the *Spitzer Space Telescope*) data covering the entire double cluster with deeper near-IR data of selected cluster regions from the Mimir camera at Lowell Observatory. With approximate completeness limits in JHK_s about 3–5 mag deeper than BK02 and Tapia et al. (1984), respectively, the 2MASS survey reaches stars with masses smaller than the limits of all optical surveys except for Keller et al. (2001) with less interference from the large line-of-sight extinction. When combined with longer wavelength (3.6, 4.5, 5.8, and 8 μm) *Spitzer* IRAC data, 2MASS and deeper near-IR surveys allow probes of disk evolution for stars with ages $\sim$10–15 Myr and masses $\gtrsim 1.3\ M_\odot$. From our analysis we hope to provide valuable input for circumstellar disk and massive cluster evolution models.

Our results provide good evidence for two populations of $\sim$13 Myr old stars in the direction of h and χ Per. In both clusters the sky surface density declines approximately inversely with distance at $\leq 20'$ from the cluster centers, which is consistent with results derived from optical data (Bragg & Kenyon 2005). At distances beyond $\sim 20'$ from the cluster centers, the surface density is consistent with the background density. CMDs indicate that nearly half of the stars within $15'$ of the cluster centers lie on a reddened 13 Myr isochrone. In regions of lower surface density $15'-25'$ from the cluster centers, however, roughly 40% of the stars lie on the same isochrone. Thus, the double cluster may be accompanied by an extensive halo population, much like the Orion star-forming region, that has roughly the same age and distance as bone fide cluster members.

While the majority of sources have photospheric IRAC colors through 8 μm, the cluster and halo population associated with h and χ Per have a small IR excess population. Disks around stars with $J \leq 13.5$ ($\sim 2.7\ M_\odot$) are extremely rare: disks around massive stars disperse by $\sim 10^7$ yr. The IR excess population is larger for fainter sources down to $J = 15.5$; disks around lower mass stars may have longer lifetimes. The IR excess population also grows progressively larger with longer IRAC wavelengths, a result consistent with an inside-out clearing of protoplanetary disks.

We begin with a description of the data and reduction in § 2 and discuss the analysis of the near-IR data in §§ 3 and 4. In § 5 we develop our technique to identify IR excess sources and use this approach to make several estimates of the fraction of IR excess sources in the cluster. We conclude with a brief summary in § 6.

2. OBSERVATIONS AND DATA REDUCTION

2.1. *Near-Infrared Ground-based J, H, and K_s Data from 2MASS*

2MASS is an all-sky survey with uniform, complete photometry at J, H, and K_s (Skrutskie et al. 2006). The survey has 10 σ sensitivity for point sources with $J \gtrsim 15.8$, $H \gtrsim 15.1$, and $K_s \gtrsim 14.3$. For sources with 10 σ detections, the survey is more than 99% complete and more than 99.95% reliable, with 1 σ astrometric accuracies of at least $0.1''$ relative to the *Hipparcos* reference frame for sources with $K_s \lesssim 14$. Although the 2MASS survey used cameras with $2''$ pixels, multiple observations of each sky position yields images with a nominal resolution of $1''$.

We downloaded data for h and χ Per from the 2MASS point source catalog (PSC) using the IRSA Web interface at IPAC.[6] The catalog includes $\sim$31,000 sources with 5 σ detections within 1° of $\alpha_{J2000.0} = 2^h20^m2.9^s$, $\delta_{J2000.0} = 57^\circ5'41.7''$ ($l = 135^\circ$, $b = -3.7^\circ$), which is a point midway between the two clusters. A sky map from the 2MASS PSC clearly shows the two clusters as dense concentrations of stars (Fig. 1). There are $\sim$11,000 sources within $25'$ of either cluster center.

Figure 2 shows the magnitude and error distributions for J and K_s using stars within $25'$ of the cluster centers. At J (K_s), the number counts monotonically increase to $J = 15.5$ ($K_s = 14.8$) and then turn over. Both of these peaks are somewhat brighter than the nominal 10 σ sensitivity limits, suggesting that confusion of sources in the galactic plane or the cluster centers might limit the source counts. However, both clusters show secondary peaks at $J \approx 14.5$ and at $K_s \approx 14$. We show below that stars within the two clusters produce these peaks.

2.2. *Near-Infrared Ground-based J, H, and K_s Data from Mimir*

The relatively low spatial resolution and the shallow peaks in the JHK_s magnitude distributions of the 2MASS data prompted us to acquire additional near-IR photometry. We used Mimir, a multifunction IR instrument[7] at the f/17 focus of the 1.8 m Perkins telescope at Lowell Observatory (Table 1). Mimir uses a Mauna Kea JHK filter set and covers a $3' \times 3'$ field with $0.18''$ pixels in this configuration. The total on-cluster coverage was $\sim$144 arcmin^2 (Fig. 1). A series of flats, darks, and biases was taken at the beginning and end of each night. The telescope was dithered by $30''$ for each pointing, with a series of three 10 s exposures taken. In most cases the pointings were too crowded to construct sky frames from median filtering. Therefore, we took a series of three 10 s dithered pairs of exposures for sky frames $7'$ in right ascension and declination away from each dithered pair of on-cluster pointings.

We followed a standard image processing procedure. First, we subtracted a dark frame from each image and divided by a dark-subtracted and normalized flat field. Next we subtracted each object frame by the appropriate median-filtered sky frame. We used a custom IDL procedure to interpolate over bad pixels as well as image/detector artifacts unique to each frame. We used another custom IDL procedure (similar to `imcombine` in IRAF) to stack 10 s frames together. Up to 18 individual frames were stacked together for each pointing yielding a total integration time of $\sim$3 minutes each in a given field. We obtained longer integrations of $\sim$7 minutes for two of the fields, one each adjacent to the h and χ Per centers, typically improving the completeness limits by $\sim$0.3 mag. Each stacked image was visually inspected for errors in offset computation and residual image artifacts.

We identified sources and extracted aperture photometry using SExtractor (Bertin & Arnouts 1996). Each potential source was convolved with a 9×9 Gaussian filter (5 pixel FWHM) and sources on image edges were removed to eliminate spurious detections. We typically used a 12 pixel diameter for aperture photometry in all bands with a tendency to use smaller apertures for K data (due to smaller point spread functions) and subtracted the background from a filtered, global background map. Sources from each dithered pair were matched to generate a final list of detections in each band.

[6] At http://irsa.ipac.caltech.edu.
[7] See http://people.bu.edu/clemens/mimir.

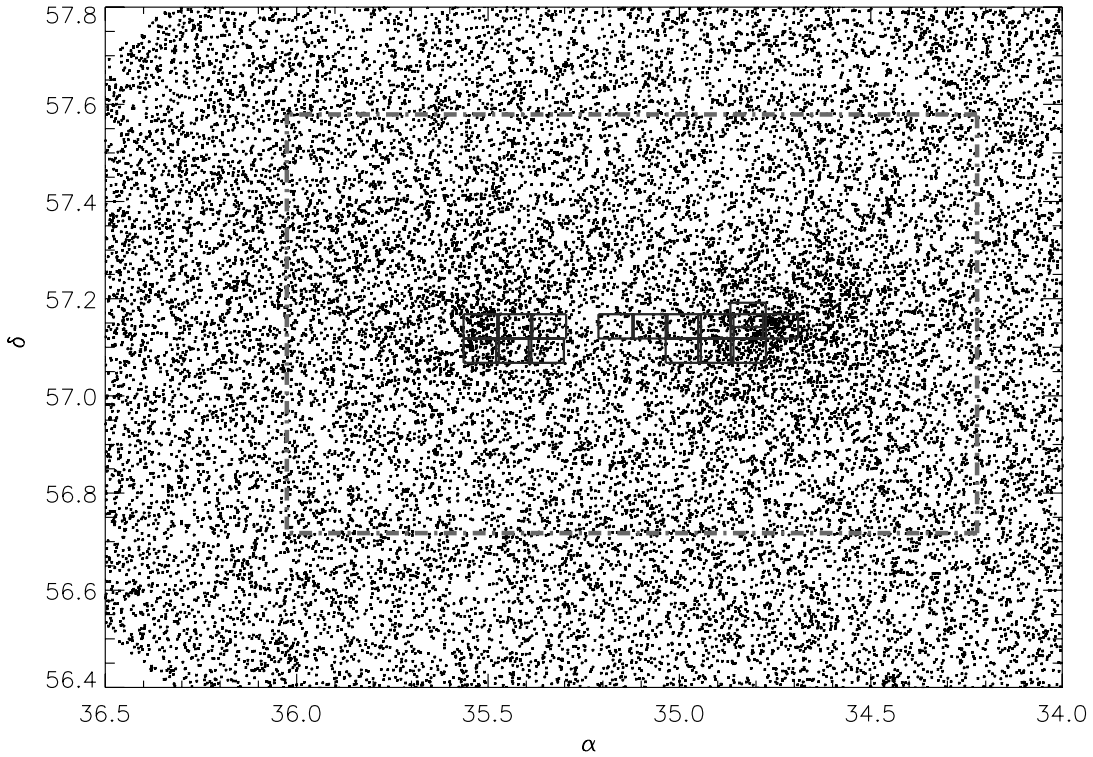

FIG. 1.—Coverage map for Mimir (*central boxes*) and IRAC (*dash-dotted line*) observations plotted over 2MASS sources in h and χ Per. The center of h Per ($2^h22^m4.3^s$, $57°8'25''$) is in the extreme right central box and the χ Per center ($2^h22^m4.3^s$, $57°8'35''$) is in the two leftmost boxes. The areas covered by Mimir and IRAC are $\sim$144 arcmin^2 and $\sim$0.75 deg^2, respectively. [*See the electronic edition of the Journal for a color version of this figure.*]

To derive an absolute calibration, we matched Mimir sources with 30–40 2MASS zero-color sources on each frame. Once we established the zero point, these sources had $\lesssim$1% offset as a function of JHK_s. For redder sources, we measured a reliable offset between K (Mimir) and K_s (2MASS) of $\sim$3% on sources with $J - K \sim 1$. Applying the conversions from Carpenter (2001) to correct Mimir colors to 2MASS colors eliminated the offset. For the ensemble of Mimir sources, we estimate absolute uncertainties of $\lesssim$0.025 mag relative to 2MASS in all bands.

To derive coordinates for the Mimir sources, we relied on accurate 2MASS astrometry. Although tests with standard packages, such as WCStools, showed that the Mimir fields were well-oriented north-south and showed little distortion and rotation, the small Mimir fields made robust astrometric solutions difficult. Because our main goals for astrometry were matching 2MASS sources and estimating incompleteness, we computed J2000.0 coordinates for Mimir sources by matching several 2MASS sources per field and deriving relative coordinates using the known pixel scale. Comparisons of all Mimir sources with 2MASS counterparts yields an average positional offset of $0.8'' \pm 0.4''$, with little evidence for systematic offsets as a function of position on the Mimir detector. Although better coordinate accuracy might be possible with complete astrometric solutions for all Mimir fields, this positional uncertainty is sufficient for robust source matching even in the centers of each cluster.

Figure 3 shows the J and K_s magnitude distributions for the Mimir data. These data reach $\sim$0.5 mag deeper than the 2MASS data, with clear peaks in the counts at $J = 16$ and at $K_s = 15.5$. Of the $\sim$1000 Mimir detections, $\sim$650 sources with $J \leq 16$ have 5 σ detections in all three bands. Multiple observations of $\sim$50 sources verified these uncertainties. At the 2MASS 10 σ sensitivity limit, we recover all 2MASS sources. At this limit, the typical magnitude difference was $\delta J \approx 0.1$ mag and $\delta K_s \approx 0.15$ mag, which is consistent with the expected error distribution.

Figure 3 shows the same secondary peaks as the 2MASS data. For a cluster age of 13 Myr, a distance modulus of 11.85, the Siess et al. (2000) isochrones, and the color conversion table from Kenyon & Hartmann (1995), the peaks at $J = 14.5$ and $K_s = 14.25$ correspond to stars with masses $M = 1.6\,M_\odot$. With these assumptions, stars at the $J = 16$ limit have masses of 1.1–1.2 $M_\odot$. In § 3 we restrict our analysis of the Mimir data to those 650 sources detected at all bands.

2.3. *IRAC 3.6–8 μm Data*

We obtained observations of h and χ Per on 2004 January 18 with IRAC (Fazio et al. 2004) on *Spitzer*. The IRAC survey covers about $\sim$0.75 deg^2 centered on $\alpha_{J2000.0} = 02^h20^m29.166^s$, $\delta_{J2000.0} = +57°12'27.54''$ (Fig. 1). There is a $\sim 7'$ offset between the channel 1/3 and channel 2/4 mosaics. We used the 12 s high dynamic range mode to obtain two frames in each position, with 0.4 and 10.4 s integration times. The observation of each field was repeated with a small offset, which allowed 20.8 s integration time for each position. We identified image artifacts and cosmic-ray hits by comparing the two observations.

The data were taken during a period of above-normal solar activity. To remove cosmic rays we evaluated two approaches. First, we took the conventional steps of mosaicking and extracting sources, relying on the cosmic-ray circumvention features of the software. We used PhotVis (ver. 1.09) for source finding and aperture photometry (see Gutermuth et al. 2004). The radii of the source aperture, and the inner and outer sky annuli were $2.4''$, $2.4''$, and $7.2''$, respectively. In the second approach, we used a custom IDL routine developed by T. C. to extract sources individually from the Basic Calibration Data prior to mosaicking,

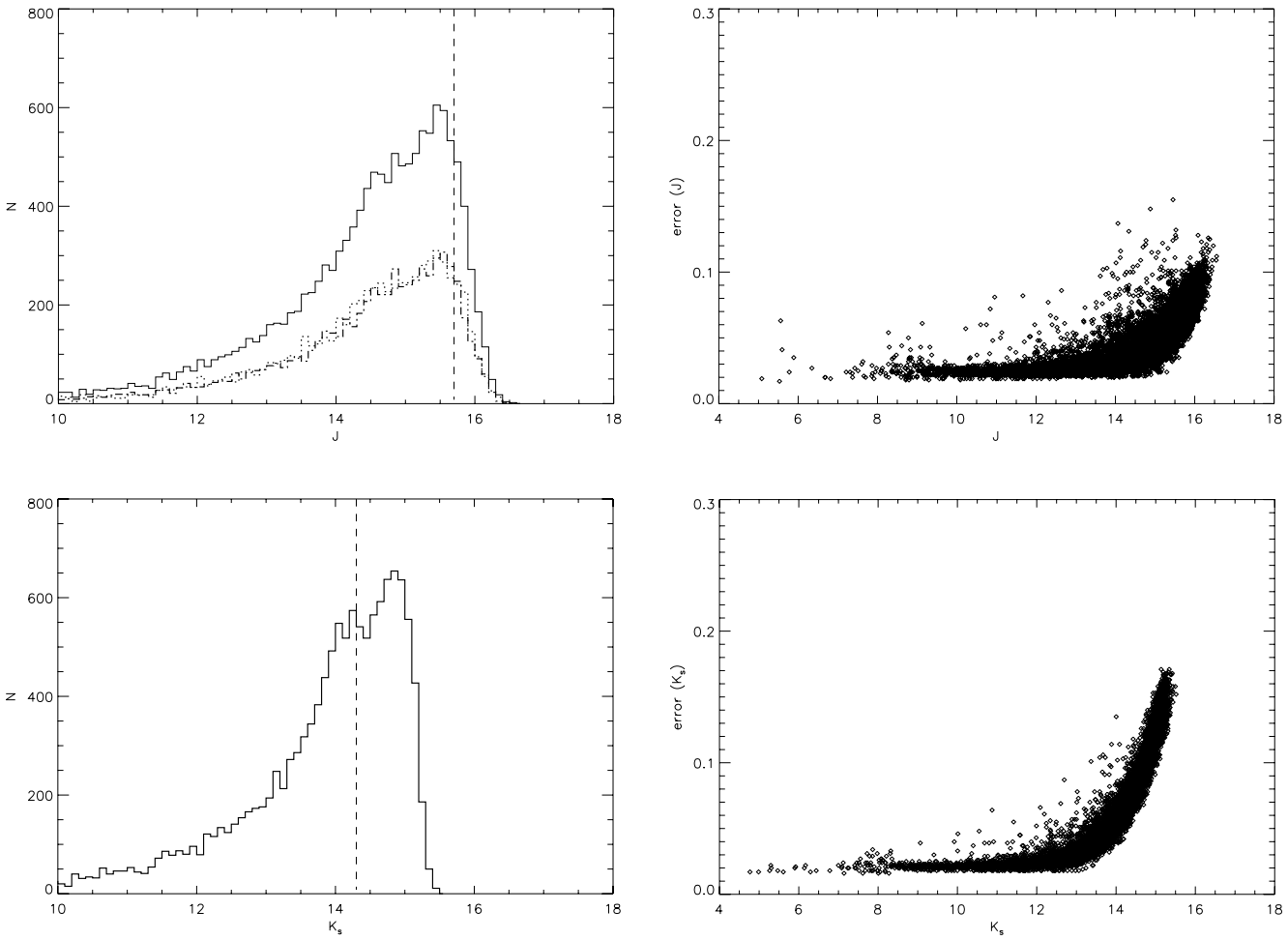

FIG. 2.—J (*top*) and K_s (*bottom*) magnitude and error distributions for 2MASS sources within 25′ of the h and χ Per centers. The dotted lines are for sources closer to h Per and the dash-dotted lines are sources closer to χ Per. The vertical dashed lines are the published 10 σ sensitivity limits for 2MASS: $J = 15.8$, $K_s = 14.3$. The small turnover near $J \sim 14.5$, $K_s \sim 14.25$ results from the large number of sources near the centers of h and χ Per that follow the ~13 Myr isochrone. The total sample is complete to $J = 15.5$ and $K_s \sim 15.0$ (~1.3 $M_\odot$) and falls to half the peak value by $J \sim 15.75$–16 and $K_s \sim 15.25$. Errors at $J = 15.5$ and $K_s = 15.0$ are less than ~0.1 and ~0.12, respectively. The distribution in K_s band shows reasonable agreement with the published 10 σ limits, while those in J fall slightly short but are reasonable through $J \sim 15.5$. We restrict the data analysis to sources with $J \leq 15.5$.

TABLE 1
MIMIR OBSERVATIONS COVERAGE

Field	α_0	δ_0	Date
1.....	2 18 56.4	57 8 35	2005 Nov 4–5
2.....	2 19 16.8	57 8 35	2005 Dec 5
3.....	2 19 37.3	57 8 35	2005 Nov 4–6
4.....	2 19 57.6	57 8 35	2005 Nov 6
5.....	2 19 16.8	57 5 35	2005 Nov 6
6.....	2 19 37.2	57 5 35	2005 Nov 6
7.....	2 19 57.6	57 5 35	2005 Nov 6
15.....	2 22 4.3	57 8 35	2005 Nov 30
16.....	2 21 43.2	57 8 35	2005 Dec 5
17.....	2 21 22.1	57 8 35	2005 Dec 1
19.....	2 20 39.7	57 8 35	2005 Dec 5
20.....	2 20 18.5	57 8 35	2005 Dec 5
22.....	2 22 4.3	57 5 35	2005 Dec 1
23.....	2 21 43.9	57 5 35	2005 Dec 1
24.....	2 21 23.5	57 5 35	2005 Dec 4
25.....	2 19 17.0	57 10 0	2005 Dec 5

NOTE.—Units of right ascension are hours, minutes, and seconds, and units of declination are degrees, arcminutes, and arcseconds.

applied array-location-dependent photometric corrections (see Quijada et al. 2004),[8] removed sources near image edges, and interpolated over pixels flagged as cosmic-ray hits/image artifacts in the first method. This approach degraded the detection limit but allowed better control of the cosmic-ray artifacts than by mosaicking alone. Source Extractor aperture photometry was performed using a 4 pixel diameter aperture; the background count level and rms was computed from the filtered, global background pixel map.

We compared the results of the two methods and examined the raw data to determine the best method for each band. This comparison included examining the number of sources with colors bluer than Rayleigh Jeans and the scatter in color-color plots, both taken as indicators of cosmic-ray effects. The source extraction prior to mosaicking provided the most reliable results in bands 1 and 2 ([3.6] and [4.5]), while mosaicking first was better in bands 3 and 4 ([5.8] and [8]). The slightly larger PSFs in the latter two bands provided enough pixels for the circumvention software to distinguish cosmic rays from real point sources. Since the intrinsic ratio of signal to noise is higher at [3.6] and [4.5] than [5.8] and [8], the degradation from extracting sources prior to mosaicking was not serious for the shorter wavelength bands.

[8] See http://ssc.spitzer.caltech.edu/irac/locationcolor.

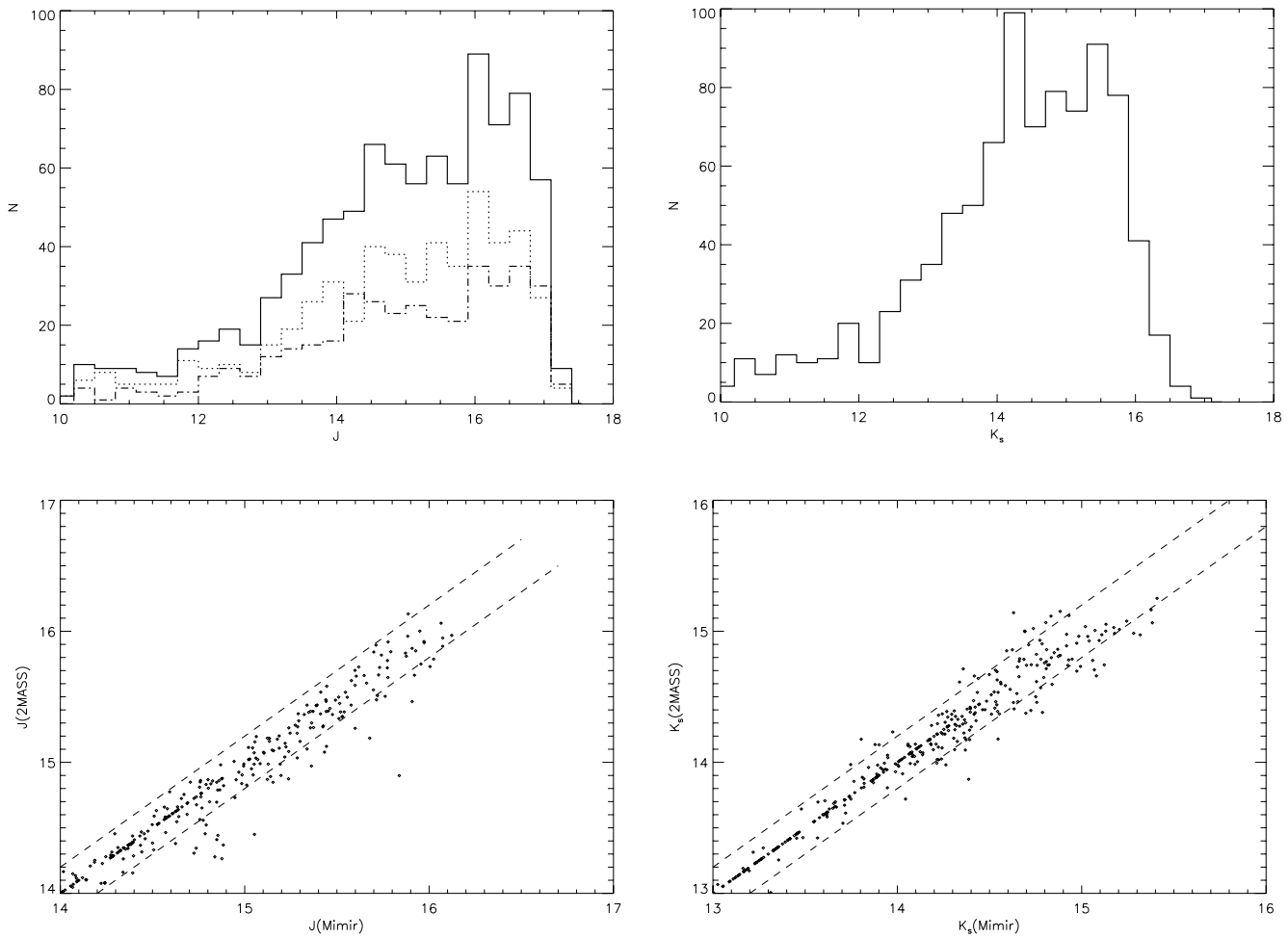

FIG. 3.—*Top left*: J distribution for h Per sources (*dotted line*), χ Per sources (*dot-dashed line*), and all h and χ Per sources (*solid line*) from Mimir. There is a small enhancement of sources near $J \sim 14.0$–14.5, which are cluster sources on a 13 Myr isochrone. The number counts in J peak at $\sim$16.0–16.25 which corresponds to stars with 1.1–1.2 $M_\odot$ at the adopted distance of h and χ Per ($\sim$2.34 kpc). However, the distribution does not fall to half its peak value until $J \sim 16.75$. We see a secondary peak at $J \sim 14.5$. *Top right*: K_s distribution for h and χ Per sources. This distribution has peaks at 14.25 and 15.5. *Bottom*: 2MASS J and K_s magnitudes vs. Mimir J and K_s magnitudes for faint 2MASS sources. Dotted lines show $\sim$0.2 mag deviations. The vast majority of sources fall within the dotted lines; the majority of sources falling outside the lines have fainter Mimir magnitudes. This is consistent with resolving binary stars, a likelihood given Mimir's higher spatial resolution. We restrict our analysis of the Mimir data to sources with $J \leq 16$.

We calibrated the photometry using large aperture measurements of standard stars obtained during h and χ Per observations, applying an aperture correction for each channel to account for the difference between the aperture sizes used for standard and h and χ Per photometry (see Reach et al. 2005 for calibration details). The brightest sources ($\leq$10th magnitude) are saturated even in the short exposure frames. Figure 4 shows the mosaic image of the [3.6] channel at low contrast. We band-merged the data using a subarcsecond matching radius to minimize the contamination of any residual cosmic-ray hits mistakenly identified as sources by the source extraction algorithms of SExtractor and PhotVis.

To remove sources that are likely AGNs or galaxies with aromatic emission, we rely on published optical data, our JHK_s data, and IRAC colors. Requiring 2MASS, Mimir, or optical counterparts eliminated most highly reddened extragalactic sources. In the IRAC bands, typical field AGN have $[4.5] > 14$ and $[4.5] - [8] \gtrsim 1.25$ (R. Gutermuth 2006, private communication); galaxies with aromatic emission lie to the right of a line from $([3.6] - [5.8], [4.5] - [8]) \sim (0, 1)$ to $\sim(1.5, 3)$ with $[4.5] - [8] \gtrsim 1$ as well as $([4.5] - [5.8], [5.8] - [8]) \sim (0, 1)$ to $\sim(1, 2.25)$ with $[5.8] - [8] \gtrsim 1$. We identify very few sources with optical/near-IR counterparts and $[4.5] - [5.8] \geq 1$ or $[5.8] - [8] \geq 1$. Thus, extragalactic sources have negligible impact on our analysis.

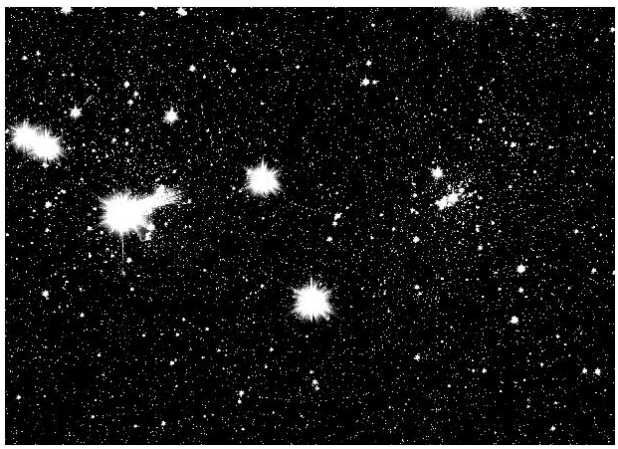

FIG. 4.—IRAC mosaic image of the h and χ Per region at 3.6 μm. The centers of h Per and χ Per are in the center right and center-left portions of the image, respectively. The contrast is set to 98%. Diffraction spikes are visible on several of the brightest sources. The *Spitzer* IRAC coverage is $\sim$1 deg^2 on the sky.

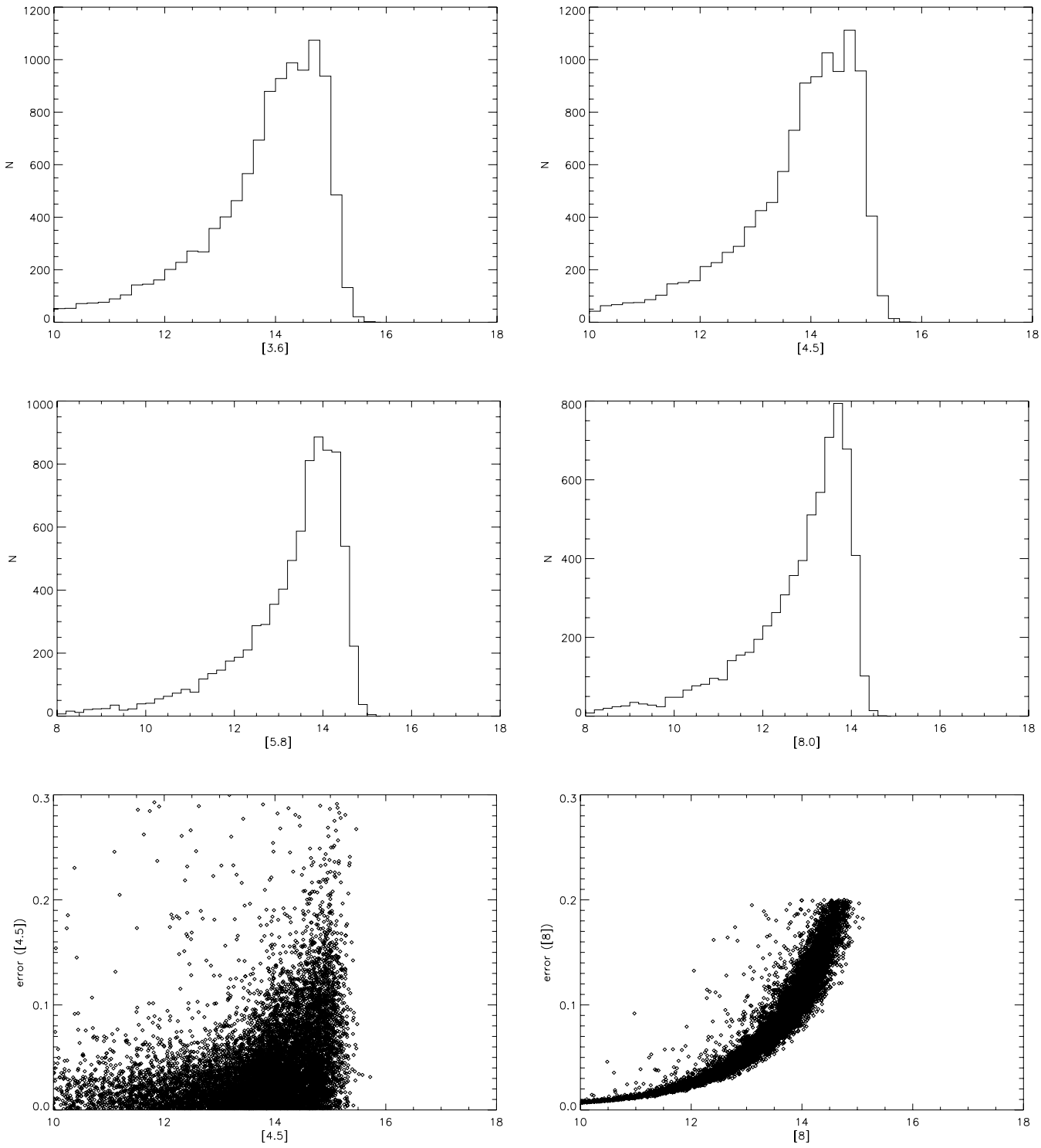

FIG. 5.—Distributions of 5 σ detections at [3.6], [4.5], [5.8], and [8]; error distributions at [4.5] and [8]. The [3.6] and [4.5] data are complete to $\sim$14.5 but have a substantial population to $m(3.6,\ 4.5) \sim 15$. The [5.8] data are complete to $\sim$14.25 with a substantial population to $\sim$14.5. The [8] data are complete to $\sim$13.75 and falls below half the peak value by $\sim$14.5. The vast majority of sources in [4.5] have errors $\leq$0.15 to $m(4.5) = 15$; sources in [8] have errors $\leq$0.2 to $m(8) = 14.5$.

Figure 5 shows magnitude distributions for the four IRAC bands and error distributions for [4.5] and [8]. At [3.6] and [4.5], the distributions have a monotonic rise to $[3.6] \approx [4.5] \sim 14$, a broad plateau at $[3.6] \approx [4.5] \sim 14$–15, and a sharp drop at $[3.6] \approx [4.5] > 15$. The longer wavelength IRAC bands have steeper magnitude distributions and brighter magnitudes with peak count levels ($[5.8] \sim 14.25$ and $[8] \sim 13.75$). The errors shown in the IRAC bands demonstrate that the average photometric uncertainty is well below 0.2 ($\sim 5\,\sigma$) at least through $[4.5] = 15$ and $[8] = 14.5$.

As with the 2MASS and Mimir data, the IRAC data show evidence for a secondary peak in the magnitude distributions. This peak lies at $[3.6] \approx [4.5] \sim 14$ and $[5.8] \sim 13.75$. Adopting the Siess et al. (2000) isochrone and the Kenyon & Hartmann (1995) colors for main-sequence stars, the peaks at JHK_s and $[3.6] - [5.8]$ are consistent with cluster stars having masses $\sim$1.3 $M_\odot$ at a distance modulus $\approx$11.85.

Figure 6 shows our estimate of sample completeness, where we plot the ratio of sources detected in both IRAC and 2MASS

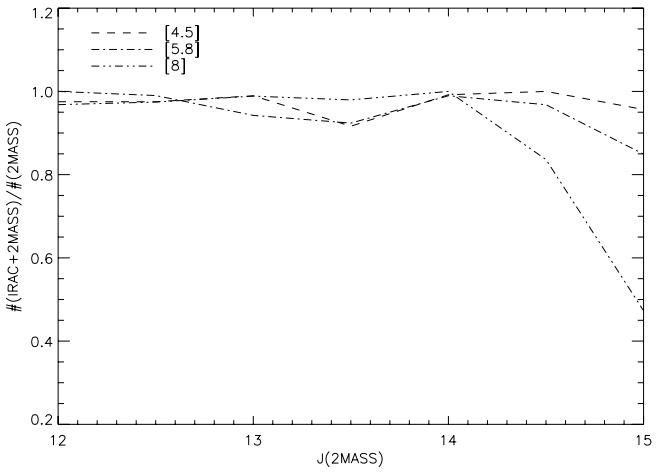

FIG. 6.—Completeness in each IRAC band as a function of 2MASS J magnitude (to $J = 15.0$). Due to the small matching radius used to combine the 2MASS and IRAC data sets, the completeness level for IRAC oscillates between 90 and 100% for $J \leq 14$. Except for the [8]-band for sources with $J = 14.5$–15, all IRAC bands are better than 85% complete. In the IRAC analysis section (§ 5) we account for completeness errors in estimating the IR excess population.

to those detected in 2MASS for each IRAC band as a function of 2MASS J magnitude (for $J \leq 15.0$). The sample oscillates between 90% and 100% complete in each IRAC band at magnitudes brighter than expected based on where the source counts peak in each band. This discrepancy, most noticeable in the [4.5] band, is due to the very small matching radius employed in combining the 2MASS and IRAC data sets, not photometric errors. If the matching radius is increased, the completeness level in the IRAC bands increases at the expense of larger cosmic-ray contamination. Because our goal is to estimate the fraction of sources with small IR excesses, we prefer to analyze a smaller sample with more robust colors. When the $K_s - [\mathrm{IRAC}]$ colors are analyzed in § 5, we consider the effect that uneven sample completeness has on our estimates of the IR excess population. Table 2 lists our photometry from 2MASS and IRAC.

3. GROUND-BASED JHK_s DATA ANALYSIS

To make reliable estimates for the fraction of cluster members with IR excesses, we must (1) derive the fraction of stars in either cluster, (2) derive robust criteria for defining an IR excess, and (3) combine the two criteria into clear estimates for the excess fraction. In this section we consider two methods for estimating the fraction of stars within each cluster, number counts, and model isochrones. The first method measures the number of stars in the clusters relative to the stars in the background population. Model isochrones allow us to estimate the fraction of stars with magnitudes and colors that are consistent with the magnitudes and colors of stars on a 13 Myr isochrone (S02). Both approaches yield similar results.

With probabilities for cluster membership established, we then consider whether any cluster stars have near-IR excesses. These data demonstrate that the vast majority of sources brighter than the completeness limits have colors consistent with photospheric colors at 1–2 μm. Thus, we find no evidence for near-IR excess sources in h and χ Per for $J \leq 15.5$, which correspond to cluster stars with masses $\gtrsim 1.3\ M_\odot$.

3.1. *2MASS Archival JHK_s Data: Density Distribution and Cluster Membership*

3.1.1. *Density Distribution of Sources on the Sky*

To investigate spatial inhomogeneities and other structure, we computed the projected sky surface density of stars, a standard approach for deriving the properties of star clusters (e.g., Binney & Tremaine 1987). We restrict our analysis here and in § 3.1.2 to sources brighter than $J = 15.5$. To derive the surface density of stars (Fig. 7, *top*), we counted stars in $1.5' \times 1.5'$ bins, displaying the density in 10% increments from 0%–90% of the peak surface density of 15 arcmin^{-2} in the center of h Per. This surface density is higher than the $\sim$7–8 arcmin^{-2} peak found by BK05, who were restricted to sources with spectral types earlier than A5. Based on J magnitude to spectral-type conversions using the Siess et al. (2000) isochrones and preliminary MMT Hectospec spectroscopy (T. Currie et al. 2007, in preparation), our population includes sources with spectral types earlier than $\sim$K0.

Aside from the strong peaks, each cluster has considerable small-scale structure. BK05 report a kidney-shaped isodensity contour in χ Per, a fairly symmetric inner core surrounded by a rectangular isodensity contour in h Per, and other structures $\sim 5'$–$10'$ from the cluster centers. With the deeper 2MASS data, these structures are clearly visible at $\sim$40%–60% of the peak density and well above the median background level of $\sim$2.7 arcmin^{-2}. The mean level is $\sim$2.8 arcmin^{-2}, and the background noise fluctuates by $\sigma \sim 0.65$ arcmin^{-2}.

Other asymmetric structures are also apparent $\sim 10'$–$15'$ from the cluster centers, which may suggest that both clusters are asymmetric on large scales, $\sim$10 pc at a distance of 2.34 kpc. However, features $\gtrsim 15'$–$25'$ from the cluster centers have amplitudes comparable to the noise level and thus might not be real. Deeper near-IR data could verify the existence of lower amplitude structure.

The bottom panel of Figure 7 shows the radial surface density plots derived from the two-dimensional map, using $1'$ wide half-annuli (facing away from midway point of h and χ Per). In both clusters the surface density drops rapidly from $\sim 2.5'$ to $10'$ and then slowly merges into the apparent background level $\sim 30'$ from the cluster centers. The surface density reaches the median background density level of 2.7 arcmin^{-2} ($\sigma = 0.278$ arcmin^{-2}; $J \leq 15.5$) $\sim 20'$–$25'$ away from the h and χ Per centers at $2^{\mathrm{h}}18^{\mathrm{m}}56.4^{\mathrm{s}}$, $57^\circ 8' 25''$ and $2^{\mathrm{h}}22^{\mathrm{m}}4.3^{\mathrm{s}}$, $57^\circ 8' 35''$, respectively (BK05). Although the clusters clearly are not symmetric, we

TABLE 2
h AND χ PERSEI DATA

α	δ	J	H	K_s	[3.6]	[4.5]	[5.8]	[8]	$\sigma(J)$	$\sigma(H)$	$\sigma(K_s)$	σ([3.6])	σ([4.5])	σ([5.8])	σ([8])
34.9281.....	56.9391	14.394	13.875	13.691	13.613	13.619	13.451	13.583	0.034	0.038	0.049	0.003	0.428	0.07	0.118
35.0360.....	56.8215	14.229	13.654	13.656	13.517	13.562	13.883	99.0	0.035	0.042	0.048	0.039	0.056	0.098	99.0
35.0483.....	57.0313	14.516	13.983	13.857	13.752	13.781	13.771	13.563	0.034	0.037	0.057	0.006	0.017	0.104	0.124
35.0523.....	56.7621	12.421	12.001	11.922	11.816	11.844	11.920	11.903	0.024	0.030	0.023	0.057	0.005	0.022	0.030
35.1106.....	56.8819	8.795	8.049	7.836	8.324	7.9730	7.787	7.731	0.018	0.024	0.018	0.014	0.168	0.002	0.003.

NOTE.—Table 2 is published in its entirety in the electronic edition of the *Astrophysical Journal*. A portion is shown here for guidance regarding its form and content.

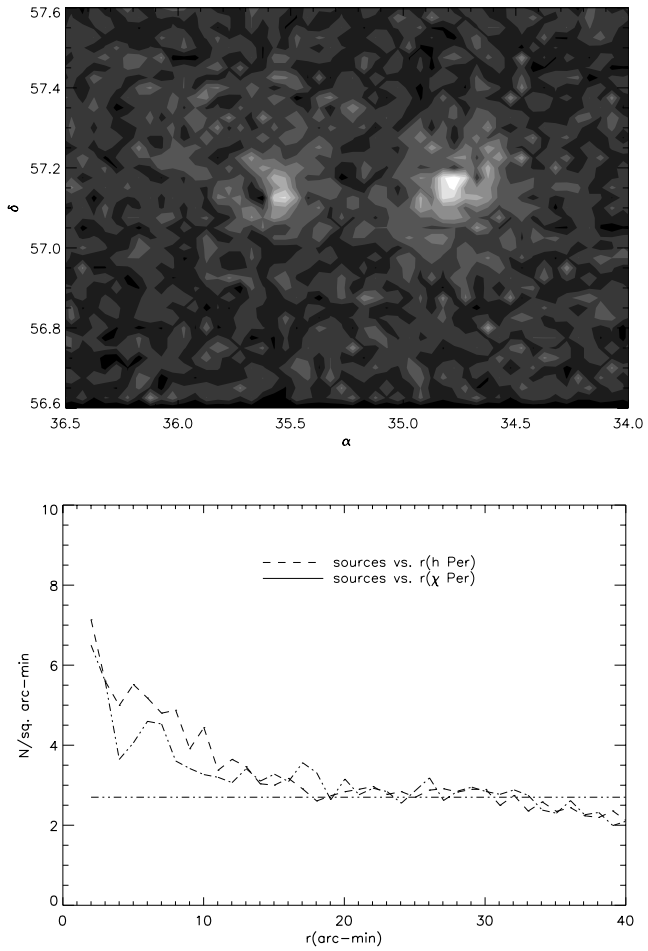

FIG. 7.— *Top*: Spatial plot of the star surface density for sources with $J \leq 15.5$ from 0% to 90% in increments of 10%. The centers of both h and χ Per (*right and left peaks*, respectively) are clearly visible and are separated by about $\sim 26'$. The clusters are $\sim 20'-30'$ across with substantial asymmetries, most notably close to the χ Per core at slightly larger declinations. *Bottom*: Radial density plot of sources with $J \leq 15.5$. The counts reach the median background density (~ 2.7 arcmin^{-2}; *dash-two dotted line*) by $\sim 15'-25'$ away from both h Per and χ Per.

can derive a reasonable estimate of the fraction of stars within the clusters by integrating the surface density above this background level. This approach yields a cluster population of ~ 2000 stars, $\sim 35\%$ of the total population within $15'$ of the cluster centers.

Although the median background level is reached $\sim 15'-20'$ there is a small gradient in the radial surface density profile from $\sim 10'-35'$ (e.g., to the limit of our sample), although no clear general gradient across the field along constant right ascension or declination. There are also is at least one region beyond $10'$ from either cluster center (from $\sim 12'$ to $20'$ away from χ Per) that may extend above its surroundings background level on scales larger than size scale of the background fluctuations. This behavior motivates us to investigate the stellar content within the "background" (beyond $\sim 15'$ from the cluster centers). Thus, we now compare the CMDs of the cluster-dominated and low-density regions.

3.1.2. *Possible Evidence for a Halo Population of $\sim 10^7$ yr Old Sources in the Vicinity of h and χ Per*

With no evidence for a significant age spread (S02) or patchy extinction (BK05) across the clusters, we can use the cluster's isochrone to constrain cluster membership. We construct $V/V-J$ and $J/J-H$ CMDs, using data from S02 and 2MASS. For both CMDs, we adopt an age of 13 Myr for the cluster (S02) using theoretical isochrones from Siess et al. (2000). For the $J/J-H$ diagram we also used pre-main-sequence tracks from Bernasconi (1996) for comparison, which show excellent agreement. To compute the cluster reddening, S02 restricted their analysis to the cluster nuclei and found a median reddening of $E(B-V) \sim 0.56$. Using a larger spatial sample of sources, BK05 computed a slightly smaller $E(B-V)$ of ~ 0.52. Since the larger spatial sample of BK05 is more similar to ours, we consider this estimate more appropriate for our sample and adopt it. This choice has negligible bearing on our results, since the reddening is low and yields an age within $1\,\sigma$ of S02's value (Bragg 2004). Converting from optical to infrared extinction via Bessel & Brett (1988) yields $E(J-H) \sim 0.185$ for $E(B-V) \sim 0.52$.

If the clusters have a small spread in age, the fraction of stars identified as being on the 13 Myr isochrone should be similar to the $\sim 35\%$ estimate derived from the number counts in § 3.1.1. For objects with $J \leq 14.5$, the $V/V-J$ diagram provides an efficient method to test for cluster membership. The S02 V data have corresponding 2MASS J limits of ~ 14.5; the diagonal slope (see Fig. 8, *top panels*) of the isochrone on $V/V-J$ allows good detection of blue, early spectral type (typically) background, nonmember sources and very red, foreground nonmembers. For objects with $J > 14.5$, the V data become incomplete. However, as shown in Figure 8 (*bottom panels*), the $J/J-H$ CMD isochrone is sensitive to membership in this magnitude range and thus provides a good substitute for the optical CMD. The two CMDs are used together to identify sources of the same age and distance of h and χ Per brighter than $J = 15.5$. We divide our sample into two main populations: an "on-cluster" population corresponding to sources within $15'$ of the cluster centers and a low-density population for sources between $15'$ and $25'$ away. We chose $15'$ for the first population because it corresponds to $\sim 3-4$ cluster core radii (BK05). Based on our density distribution analysis, this distance corresponds to the point at which the typical stellar density begins to approach the median background level. The $25'$ outer radius for low-density regions is chosen primarily because it fully samples our entire IRAC coverage. According to the modified Hubble law distribution ($\rho \sim r^{-2}$) of cluster members, the cluster density ~ 4 core radii away should be $\sim 6\%$ of the peak density. If the number of stars in a circle of diameter $1'$ at the center is N, an annulus of $1'$ width at $15'$ should have roughly $(4-5)N$ stars in the cluster and roughly 25–30 times that many in the "background." The fraction of stars in the cluster beyond $15'$ to $25'$ should be over twice as small ($\rho \sim 0.01-0.03\rho_{\rm peak}$). Therefore, if h and χ Per sit in a background of nonrelated field stars, the low-density regions beyond $15'$ will be dominated by sources of different ages and distances than sources in h and χ Per. The density of sources tracking the isochrone should be *far* larger within $15'$ than outside $15'$.

The $V/V-J$ diagram for sources within $15'$ of the h and χ Per cluster centers (Fig. 8, *top left*) clearly shows a distribution of sources tracking the 13 Myr isochrone for $V = 12-16$. The isochrone slightly bends at $V \sim 15-15.5$. Foreground sources are clearly visible above the isochrone. Figure 8 (*bottom left*) shows the $J/J-H$ CMD for all sources within $15'$. Sources with $J \leq 14.5$ track the reddened isochrone well, except for some sources with $J-H \gtrsim 0.5$, which are probably foreground M dwarfs or background M supergiants. The isochrone "bends" horizontally at $J \sim 14.5$. Almost all sources to $J = 15-15.5$ fall along the 13 Myr isochrone or are redder. Although many sources with $J \geq 15.5$ may follow the isochrone, the larger errors ($\sigma > 0.1$) and increasing population of blue sources make it hard to measure the cluster population. Thus, we restrict our analysis to stars with $J \leq 15.5$.

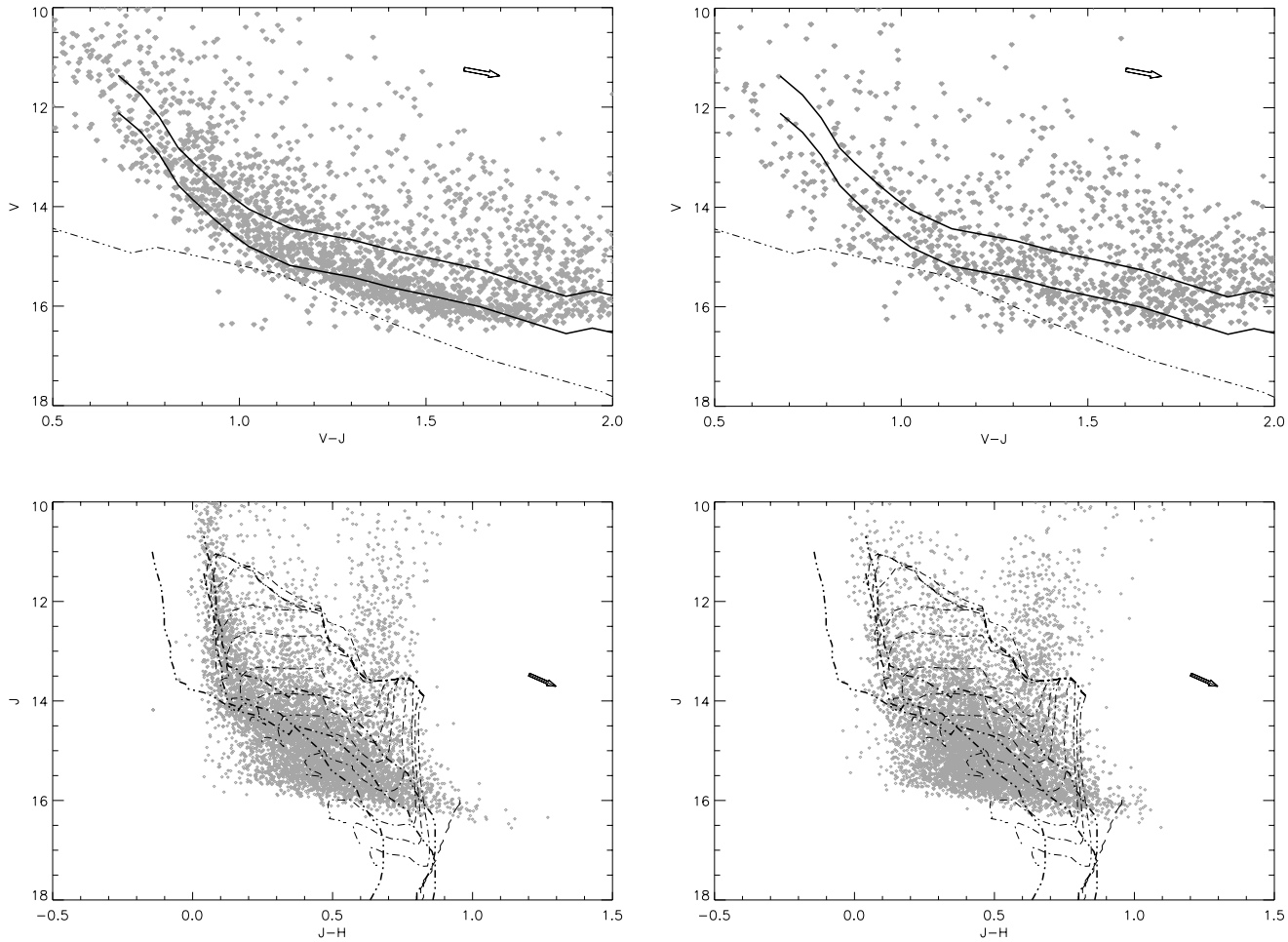

FIG. 8.— $V/V-J$ (*top*) and $J/J-H$ (*bottom*) CMDs of the 2MASS and S02 sources with $\sigma \leq 0.2$ for sources within 15′ (*left*) and those between 15′ and 25′ (*right*) from the h and χ Per cluster centers. Overplotted are the Siess et al. (2000) isochrones for a 13 Myr cluster (*dash-two-dotted line*) with a "reddened" isochrone [$E(B-V) \sim 0.52$: *solid line*] and appropriate reddening vectors [$A_V \sim 1.4E(V-J)$; $A_J \sim 2.49E(J-H)$]. For the $J/J-H$ diagram, the reddened pre-main-sequence tracks for 0.8–7 $M_\odot$ stars from Bernasconi (1996, *dot-dashed line*), and those for lower mass stars from Baraffe et al. (1998, *long dashes*) are also plotted. Sources between 15′ and 25′ away from the cluster centers appear to contain a population tracking the isochrone by $V \geq 14.5$ and $J \geq 13.5$. [*See the electronic edition of the Journal for a color version of this figure.*]

The top right panel of Figure 8 shows the $V/V-J$ diagram for sources both 15′–25′ from each cluster center and greater than 15′ from both centers. While sources appear quite scattered around the isochrone for $V \leq 14$, there is a significant population of sources between the two isochrones (for single and binary stars) for $V = 14$–16.5. There are also many sources between the corresponding isochrones in the J, $J-H$ CMD (Fig. 8, *bottom right*). From analysis of the projected radial density distribution, regions $\geq$15′ from either center should contain mostly background or foreground, nonmember sources. The fact that the fainter of these sources loosely follow the 13 Myr isochrone for the cluster suggests that there may be a larger region of enhanced formation of low-mass stars in the same general direction. This behavior would be similar to the situation with the Orion cluster, for example.

We now quantify the fraction of sources in the h and χ Per 2MASS coverage that are consistent with cluster membership by counting the number of stars that are, within photometric errors, lying on the $V/V-J$ and $J/J-H$ isochrones and the number lying outside them. We require that sources be within 0.3 mag ($\sim 5\,\sigma$ added in quadrature) of the isochrone to count as members. This procedure neglects colors expected for unresolved binaries, which would increase the source brightness for a given color. We compare the number of h and χ Per sources less than 15′ away from either cluster core and the number between 15′ and 25′ away. Sources $\geq$15′ from one cluster and $\leq$15′ from the other cluster were not counted.

From the $V/V-J$ diagram, $\sim$33% of sources within 15′ of the cluster centers have a CMD position consistent with cluster membership ($\sim$767 with $J \leq 14.5$). In the sample of stars at 15′–25′ from the cluster centers, $\sim$23% lie in a similar zone on the CMD. About $\sim$47% of sources within 15′ have a CMD position consistent with a 13 Myr isochrone ($\sim$2600 sources with $J \leq 15.5$) on the $J/J-H$ diagram. Stars near the 13 Myr isochrone between 15′ and 25′ away from either center make up a comparable fraction $\sim$41%. If we group the two populations together, $\sim$44% of the $\sim$ 11,000 sources are of the same age, distance, and reddening as h and χ Per. Therefore, within 25′ of the cluster centers the population of sources with $J \leq 15.5$ lying near a 13 Myr isochrone is $\sim$4700: $\sim$2500 closer to h Per and $\sim$2200 closer to χ Per. Estimates for the fraction of 13 Myr sources from the $J/J-H$ diagram are comparable ($\sim$27% and 20% for $\leq$15′ and 15′–25′, respectively) to those from the $V/V-J$ diagram in the appropriate limit ($J \leq 14.5$): the lower fractional memberships for $J \leq 14.5$ are likely caused by a high number of foreground K and M stars and background M supergiants. Thus, to within $\sim$10%–15%, both the $V/V-J$ ($J \leq 14.5$) and $J/J-H$ ($J \leq 14.5$, 15.5) CMDs predict comparable estimates of the percentage 13 Myr sources at the distance of h and χ Per. Furthermore,

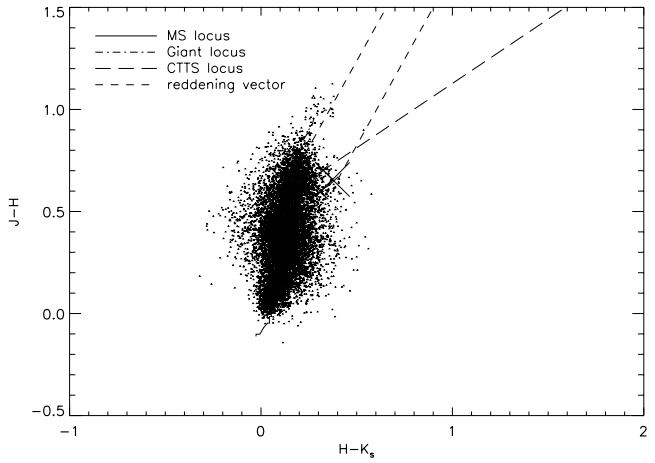

FIG. 9.—$J - H$ vs. $H - K_s$ colors from 2MASS for 11,048 sources with $J \leq 15.5$. Overplotted are the classical T Tauri (Meyer et al. 1997) and giant loci (Kenyon & Hartmann 1995). Crosses represent the change in colors that a source with photospheric $J - H/H - K_s$ colors of ~0.55/0.1 would have if a 1500 K blackbody (from a circumstellar disk) contributed 5%, 25%, and 50% of the total flux at 3.6 μm.

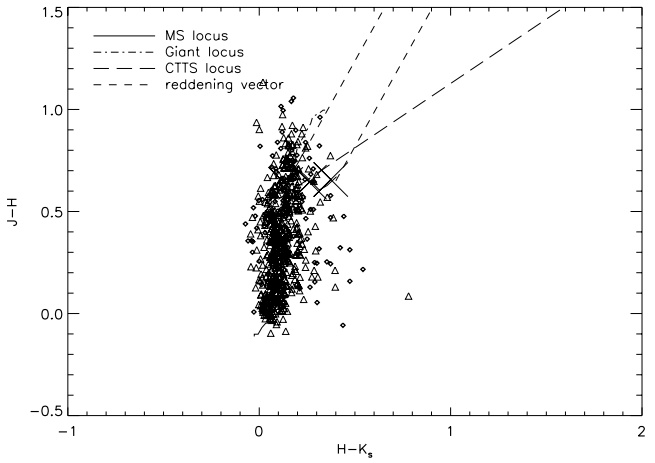

FIG. 10.—$J - H$ vs. $H - K_s$ colors from Mimir complete for 657 stars with to $J = 16$ (~1.1 $M_\odot$, $d \sim 2.34$ kpc). Filled diamonds represent sources detected at the 10 σ ($\sigma \leq 0.1$) level in all bands; triangles represent sources with errors less than $\sigma = 0.2$ in the three bands. Overplotted are the classical T Tauri (Meyer et al. 1997) and giant (Kenyon & Hartmann 1995) loci.

the percentage of sources lying on the 13 Myr isochrone in the low-density regions (15′–25′) and high-density regions (≤15′) are consistent within ~10% of one another. If the "background" were dominated by foreground and background sources, then the percentage of 13 Myr sources in the high-density regions should be much larger than in the low-density regions.

It is difficult for a random distribution of foreground/background stars with a wide range of ages and spectral types to mimic a $\sim 10^7$ yr isochrone, so we conclude that at least *some* of the background population includes young stars with nearly identical ages and distances as those in the two clusters. From the poorer definition of the cluster along the isochrones in the right panels of Figure 8, these stars may be distributed over a few hundred parsecs along the line of sight, centered roughly on the clusters and probably associated with them. The population of sources roughly tracking the 13 Myr isochrone in $J/J - H$ only slowly disappears by ~60′ from the cluster centers (not shown), suggesting a diameter of about 100 pc. However, while it may be possible that the halo population extends to ~60′ away from h and χ Per, carefully quantifying its disappearance, particularly for the upper main sequence at ~13 Myr, requires wider angle imaging and deep spectroscopy and is beyond the scope of this paper.

The existence of a halo population of stars at about the same age, distance, and reddening as those within the cores of h and χ Per was considered by Schild (1967) based on spectroscopy and photometry of the brightest sources; S02 also noted that, to $V \sim 16$, the optical colors of bright sources beyond 5′ of either cluster center and those within 5′ of either cluster center appeared quite similar. Our result, probing stars slightly fainter than those studied by S02 and over larger spatial area, is broadly consistent with both of these references. For the rest of the paper, we shall restrict our analysis to sources within 25′ of the cluster centers. We use the $V/V - J$ and $J/J - H$ diagrams to identify sources within this radius that appear to have the age, distance, and reddening of h and χ Per.

3.2. *JHK_s Color-Color Diagrams from 2MASS and Mimir*

Now we investigate the near-IR 2MASS colors of all sources within 25′ of the cluster centers (~11,000) with $J \leq 15.5$. The $J - H/H - K_s$ color-color diagram is shown in Figure 9 with the main-sequence locus, giant locus, classical T Tauri locus, and reddening bands. Stars with $J - H \approx 0.0$–0.25 and $H - K_s \approx 0.0$–0.3 will include Be stars with near-IR excess from optically thin gas (Dougherty et al. 1991, 1994). Excesses around later type stars with $J - H \geq 0.3$ and $H - K_s \geq 0.35$ are more likely to have near-IR excess emission from warm dust. The vast majority of sources have photospheric colors. Sources off the locus are distributed evenly on both sides, suggesting that photometric errors may be responsible for any $H - K_s$ "excess." To characterize the population more accurately and (later) search for near-IR excess sources at $H - K_s$ we rely on Mimir data with deeper completeness limits at JHK_s.

We analyze Mimir sources with $\sigma \leq 0.2$ and $J \leq 16$. Figure 10 shows the $J - H/H - K_s$ color-color diagram for all sources in the Mimir survey. The vast majority of sources fall along the main-sequence locus. Figure 11 shows data separately for h Per and χ Per; h Per has more sources with a slight $H - K_s$ excess for small $J - H$ colors (≤0.3). The horizontal spread in color is noticeably smaller for sources with $\sigma \leq 0.1$. Many sources have colors consistent with disk excess emission ($H - K_s \sim 0.4$ or redder). However, restricting ourselves to sources that may be cluster members based on the $J/J - H$ diagram, the IR excess population from $H - K_s$ through $J = 15.5$–16 is *extremely* small: less than ~1%.

4. IRAC ANALYSIS: 2MASS − [IRAC] COLORS AND IRAC-ONLY COLORS

To learn whether excesses are more common at longer wavelengths we consider the IRAC data. Restricting our analysis to sources within 25′ of the cluster centers, we have ~7000 sources with 5 σ detections at [3.6] and [4.5]; ~5000 of these have 5 σ detections at [5.8] and [8.0]. To minimize contamination due to large errors, we restrict this sample to the sources with K_s, [IRAC] ≤ 14.5.

The $H - K_s/K_s - [3.6]$ and $H - K_s/K_s - [4.5]$ diagrams are shown in Figure 12. In each plot nearly all sources have photospheric colors, with $K_s - [3.6]$, $[4.5] \approx 0.0$–0.3 or 0.4. Sources with $K_s - [3.6]$, [4.5] much larger than 0.3–0.4 are much redder than normal stellar photospheres. The number of "red" sources is larger at [4.5] than at [3.6] and suggests the existence of an IR excess population in h and χ Per.

Figure 13 shows the $[3.6] - [4.5]/[4.5] - [5.8]$ and $K_s - [3.6]/K_s - [5.8]$ color-color diagrams. In previous studies of IRAC colors of pre-main-sequence stars (e.g., Hartmann et al. 2005), a

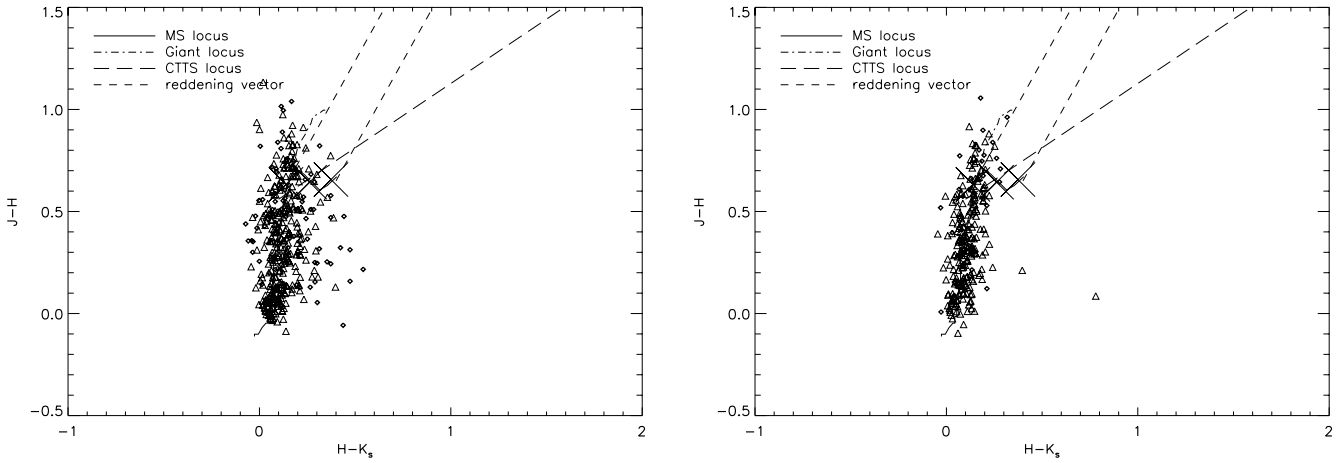

FIG. 11.—$J - H$ vs. $H - K_s$ colors from Mimir for h Per (*left*) and χ Per (*right*). The symbols are the same as in previous plots.

division between class II and class III T Tauri stars occurs roughly at $[4.5] - [5.8] \sim 0.2$–0.25. The h and χ Per color distribution has a red limit of about 0.3 resulting from the intrinsic dispersion of colors. Many sources have colors redder than this limit (K_s, $[4.5] - [5.8] \geq 0.3$). There are few sources with $[4.5] - [5.8] \leq -0.3$. The common-baseline $K_s - [3.6]/K_s - [5.8]$ diagram shows the very red population even more clearly. Photospheric sources have $K_s - [5.8] \lesssim 0.3$–0.4. The plot also suggests that there may be some sources with red colors at $K_s - [5.8]$ but not $K_s - [4.5]$, judging from the relatively larger number of sources.

The distribution at $[5.8] - [8]$ (Fig. 14, *left*) continues to show a very gradual, as opposed to abrupt, transition in colors from photospheric ($[5.8] - [8] \leq 0.2$) to very red ($[5.8] - [8] \geq 0.4$) (see Allen et al. 2004). In Hartmann et al. (2005) there are very few sources with $[5.8] - [8] = 0.25$–0.4. The lack of any gap in h and χ Per is likely due to larger photometric errors at [8]. The same plot for 10 σ sources (Fig. 14, *right*) shows a much smaller dispersion in $[5.8] - [8]$ colors containing sources with $[5.8] - [8] = 0.25$–0.4. There is also a substantial number of 10 σ detections with $[5.8] - [8] \geq 0.4$.

Constructing colors from the 2MASS K_s band and IRAC bands at [5.8] and [8] provides the clearest evidence for an IR excess population in h and χ Per. Figure 15 shows the $K_s - [3.6]/K_s - [8]$ color-color diagram, which is our closest analog to the $K - L/K - N$ diagram used by Kenyon & Hartmann (1995) to distinguish class II and III T Tauri stars in Taurus. Photospheric sources appear to have $K_s - [8] \leq 0.4$; with $K_s - [8] \gtrsim 0.4$ there is a clear population of IR excess sources. The $K_s - [5.8]/K_s - [8]$ diagram also shows an excess population for $K_s - [5.8, 8] \geq 0.4$.

The population of very red, IR excess sources in $K_s - [\text{IRAC}]$ is statistically significant. The mean and dispersion in $K_s - [4.5]$ are $\sim -0.02 \pm 0.06$, 0.07 ± 0.1, and 0.07 ± 0.1 at $J = 12$, 14.5, and 15. For $K_s - [8]$ color these values are 0.06 ± 0.1, 0.15 ± 0.18, and 0.24 ± 0.19; the values for $K_s - [3.6]$ are similar to $K_s - [4.5]$ and those for $K_s - [5.8]$ are in between $K_s - [4.5]$ and [8]. The median colors are nearly identical in all cases. In all $K_s - [\text{IRAC}]$ colors there exists a substantial population of sources that are more than 2–5 σ redder than the mean color while a corresponding blue population does not exist. It is clear from the IRAC colors that h and χ Per harbors a significant IR excess population.

5. ANALYSIS OF THE IR EXCESS POPULATION

Now we quantify the fraction of sources with excesses from 2MASS and IRAC photometry and thus the population of sources with circumstellar disks. With no evidence for IR excess at K_s, we estimate the fraction of sources with IR excess at [4.5], [5.8], and [8], using K_s as a common short wavelength baseline, and then relate the IR excess population to intrinsic stellar properties via the 2MASS J band. The J filter should have emission dominated by the stellar photosphere, especially for sources older than 10 Myr that typically are not actively accreting. Converting from

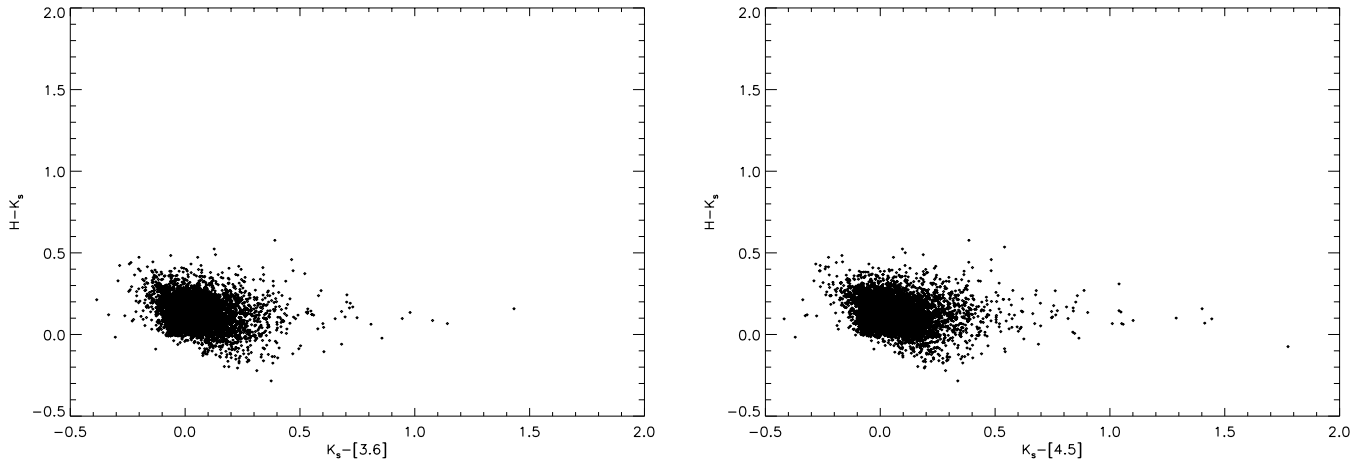

FIG. 12.—$H - K_s/K_s - [3.6]$ color-color diagram (*left*), and $H - K_s/K_s - [4.5]$ diagram (*right*). The distribution of $H - [3.6]$, $H - [4.5]$, $K_s - [3.6]$, and $K_s - [4.5]$ colors show a potential IR excess population with $K_s - [\text{IRAC}] \gtrsim 0.3$–$0.4$.

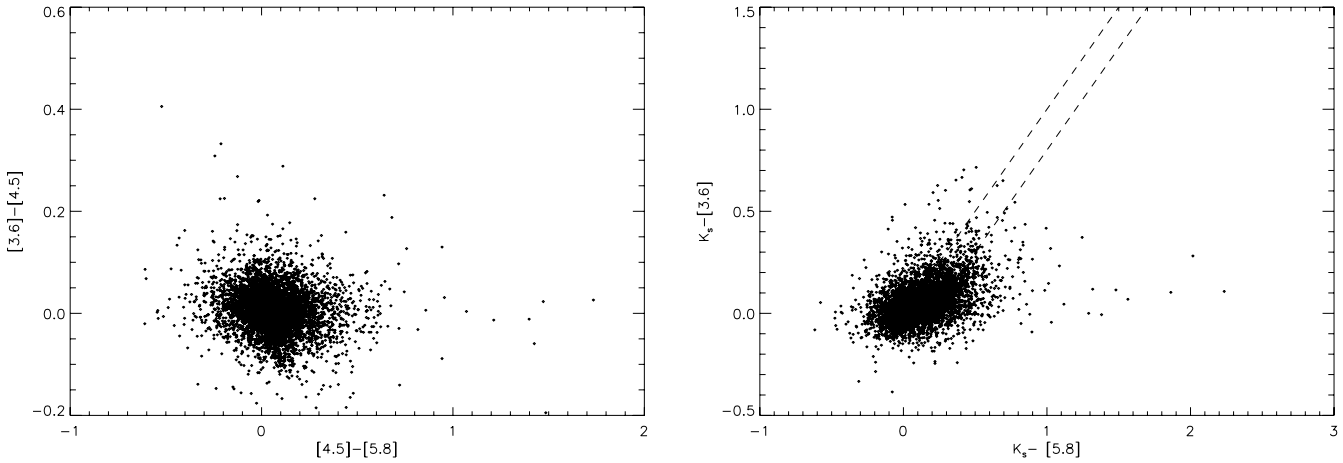

FIG. 13.—[3.6] − [4.5]/[4.5] − [5.8] (*left*) and K_s − [3.6]/K_s − [5.8] color-color diagrams (*right*) of sources with $J \geq 11$, $\leq$15.5, and $m(5.8) \leq 14.5$. In the bottom diagram the dotted lines denote sources with [3.6] − [5.8] = 0–0.3. The photospheric population appears to have a red edge [4.5] − [5.8] = 0.3 and K_s − [5.8] = 0.4. In § 5 we count sources with K_s − [5.8] $\geq$ 0.5 as IR excess candidates.

J magnitudes to stellar properties is also more straightforward than with optical filters because J is less affected by reddening. We analyze the IR excess population as a function of J in 0.5 mag bins.

In § 5.1 we describe our two methods for selecting sources as h and χ Per members. Next we describe our criteria for identifying a source as an IR excess source in § 5.2. We estimate the size of the IR excess population using a highly restrictive model for membership and IR excess identification and then using a less restrictive model. We describe both models in § 5.3.

The estimates from both the restrictive and less restrictive models show excellent agreement. The relative size of the IR excess population to the total population increases with J magnitude. Most of the IR excess sources have $J = 14$–15; very few excess sources are brighter than $J = 13.5$–14. This result implies that the frequency of disks around stars with ages 10–15 Myr is likely higher for lower stellar masses. The IR excess population is consistently larger at longer IRAC wavelengths than at shorter wavelengths: this behavior is expected if circumstellar disks clear from the inside out. At least ~4%–8% of sources with $J = 14$–15 (~2.2–1.4 $M_\odot$) have IR excess indicative of a circumstellar disk. We also identify sources that have IR excess at both [5.8] and [8]. About ~2%–3% of sources have strong IR excess at both long wavelength IRAC channels for sources as faint as $J = 15.0$.

5.1. *Sample Selection*

Our first task is to remove probable nonmembers of h and χ Per. After removing sources identified as AGNs/aromatic-emission galaxies we used the $V/V - J$ and $J/J - H$ color magnitudes to remove sources inconsistent with the 13 Myr isochrone (§ 2.3). The most restrictive, cautious approach is to use only the sources with optical photometry from S02 because the long-baseline $V - J$ color is better at identifying nonmembers than the shorter baseline $J - H$ color. For this approach we require sources lying within 0.3 mag (~5 σ errors added in quadrature) of the isochrone in V:

$$|V(\text{source}) - V(\text{isochrone})| \leq 0.3. \quad (1)$$

Thus our sources consistent with h and χ Per membership should fall within a band 0.3 mag brighter and fainter than the nominal reddened isochrone. However, the V magnitude data from S02 is complete only to ~14.5 in J. Thus restricting our analysis to optical sources eliminates stars with $J > 14.5$ or $M \lesssim 1.6\ M_\odot$.

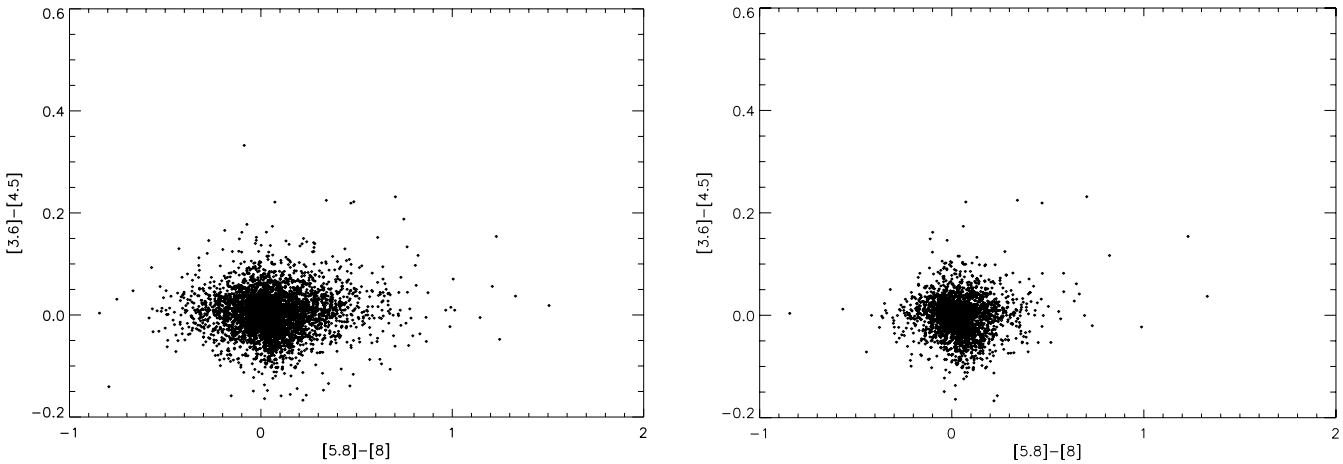

FIG. 14.—*Left*: Four-channel IRAC colors for sources within 25′ of h and χ Per centers. The population of sources in the clear "break" between class II and III T Tauri stars from 0.25–0.4 is large compared to the overall population of sources with IR excess ([5.8] − [8] $\geq$ 0.4). *Right*: Same four-channel IRAC color distribution among sources with small ($\sigma \leq 0.1$) errors in [8]. There are sources in the break between class II and III colors from [5.8] − [8] = 0.25–0.4 and excess sources beyond [5.8] − [8] ~ 0.4.

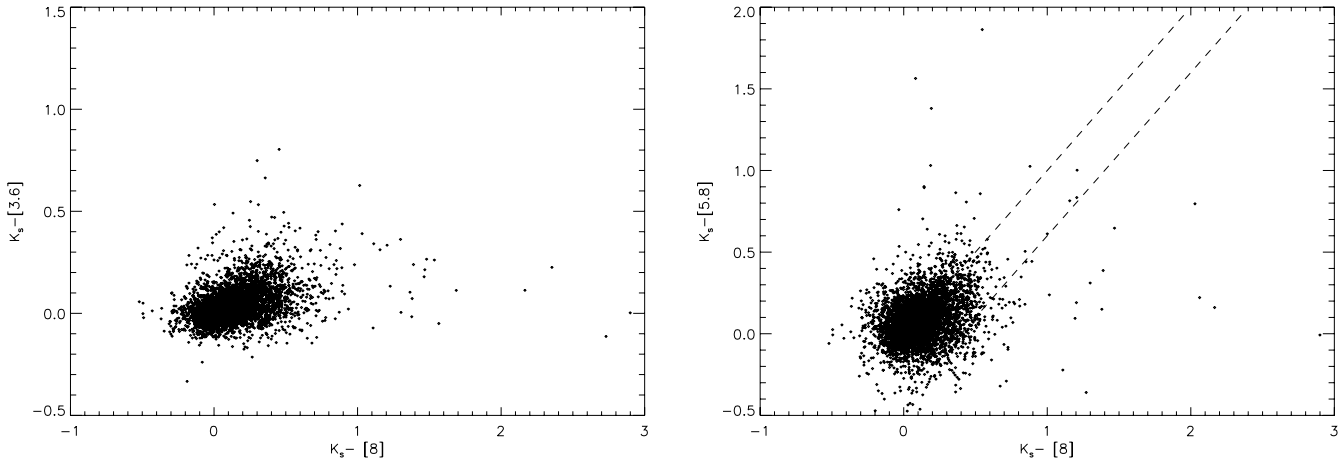

FIG. 15.—$K_s - [3.6]/K_s - [8]$ (*left*) and $K_s - [5.8]/K_s - [8]$ (*right*) color-color diagrams for sources with $J = 11$–15.5 and $[8] \leq 14.5$. The dotted lines in the bottom panel bound sources with $[5.8] - [8] = 0$–0.4. In both plots there is a red edge to the main population at $K_s - [8] \sim 0.4$ and many IR excess sources with $K_s - [8] \geq 0.4$.

A less restrictive approach uses the 2MASS $J - H$ color to identify ~13 Myr, 2.34 kpc distant stars. Sources in unresolved binary systems should be $\leq$0.75 mag too bright for their color. The faint limit, however, should be unchanged. Our criteria are then:

$$J(\text{source}) - J(\text{isochrone}) \geq -0.75, \ \leq 0.3. \qquad (2)$$

This 2MASS sample is complete to $J = 15.5$, which includes stars with $M \gtrsim 1.3\ M_{\odot}$.

5.2. *IR Excess Criteria*

A color threshold is set for a source to be considered an IR excess candidate using the 2MASS − [IRAC] color-color diagrams and Kenyon & Hartmann (1995) photometry and color table as a guide. For the [4.5] channel we use the $K_s - [3.6]/K_s - [4.5]$ diagram, for the [5.8] channel we use $K_s - [3.6]/K_s - [5.8]$, and for the [8] channel we use $K_s - [3.6]/K_s - [8]$ (Figs. 11, 12, and 14). The main distribution of sources in these diagrams has $K_s - [\text{IRAC}] \leq 0.4$. For comparison, Kenyon & Hartmann found that sources with $K - L \leq 0.3$–0.4 were typically class III T Tauri stars with weak Hα emission and little evidence of circumstellar dust at L band (see also McCabe et al. 2006, Figs. 1 and 2). According to the Siess et al. (2000) isochrones, 13 Myr sources more massive than $\sim 1\ M_{\odot}$ should also not have $K - L \geq 0.2$–0.25, assuming the extinction derived by BK05. Sources with $K_s - [\text{IRAC}] \geq 0.4$ are then likely IR excess source candidates.

To avoid defining sources with large photometric errors as excess sources, we make the additional requirement that a source's color must be redder than the absolute threshold plus the source's photometric error, σ, in the IRAC bands, or

$$K_s - [\text{IRAC}] \geq 0.4 + \sigma(\text{IRAC}). \qquad (3)$$

Fainter IRAC sources ($\sim$ 14–14.5) then typically must have $K_s - [\text{IRAC}] \gtrsim 0.5$–0.6 to be classified as excess sources. As a sanity check, we also require that the next longest wavelength IRAC band show at least a marginal excess, $K_s - [\text{IRAC}] \geq 0.3$, if a 5 σ detection was made at such a channel.

Finally, we remove potential completeness-related bias and calculate errors on the size estimates of the IR excess population. First, because the completeness limits from J through [8] vary, we apply a uniform cutoff across 2MASS and IRAC bands and restrict ourselves to sources with K_s, $[\text{IRAC}] \leq 14.5$, as the count rate for 5 σ detections at [8] falls to half-peak values by 14.5. Because sources with $K_s \sim 14.5$ have $J - K_s \sim 0.4$–0.7, we add a further restriction that sources must have $J \leq 15.0$. Estimates for the size of the IR excess population in each IRAC band are then drawn from a single population. Nominally, the errors for the IR excess fraction in each 0.5 J magnitude bin are calculated from Poisson statistics, $\sigma \sim \sqrt{\mathcal{N}}/N$, where $\mathcal{N}$ is the number of sources with IR excess and N is the number of sources in the bin with detections in 2MASS and at a given IRAC band. We retain this error estimate as an upper bound on the IR excess fraction. However, there may be sources in our coverage that are detected in 2MASS but not in IRAC and are brighter than our J magnitude cutoff. Thus, these sources would not be included in our calculation for N because of their nondetection in IRAC. This could bias our results in favor of detecting more IR excess sources and fewer photospheric sources near magnitude 14.5 and thus is another source of error.

To put a limit on this error, we calculate the number of sources in each bin detected at both J and K_s. If the IRAC sample is 100% complete, this number M should be equal to N, otherwise it will be larger. We then assume that any source in M not detected in N is not an IR excess source and divide the total number of IR excess sources by M. This procedure yields an absolute lower limit on the fraction of sources with IR excess in each 0.5 mag bin. We subtract this value from the nominal fraction to produce an error estimate due to sample completeness. The larger of the two errors, the Poisson error and the completeness error, is chosen as the lower bound on the IR excess fraction.

5.3. *Two Models for Analyzing the IR Excess Population*

Equipped with our two approaches for sample selection, our method for identifying an IR excess source, and our brightness cutoffs in 2MASS and IRAC, we now describe our two models for analyzing the IR excess population. The models, summarized in Table 3, are as follows:

Model 1 (restrictive): We require that sources have optical counterparts from S02 and that they are within 0.3 mag of the 13 Myr $V/V - J$ isochrone (eq. [1]). We require that IR excess candidates fulfill the condition set in equation (3). We investigate the IR excess population at [4.5], [5.8], and [8] for sources with $J \leq 14.5$. Errors for the size of the IR excess population in all models assume Poisson statistics.

Model 2 (less restrictive): We require that sources have near-IR colors consistent with the 13 Myr $J/J - H$ isochrone as described by equation (2). We require that the IR excess candidates fulfill

TABLE 3
MODELS FOR ESTIMATING THE IR EXCESS POPULATION

Model	Membership Determination	Membership Cutoff	J Cutoff
1 (more restrictive)	$V/V-J$ colors[a]	$\lvert V-V(\text{isochrone})\rvert \leq 0.3$	14.5
2 (less restrictive)	$J/J-H$ colors[b]	$J-J$ (isochrone) ≥ -0.75, ≤ 0.3	15.0

NOTES.—Brief description of the two models for identifying IR excess sources. In the first model we require that sources have optical data from S02 and use the $V/V-J$ diagram to constrain cluster membership. We analyze sources to $J = 14.5$. In the second model we use the $J/J-H$ diagram from 2MASS to constrain cluster membership. We analyze sources to $J = 15$. The membership cutoff refers to how far away a source can be from the 13 Myr isochrone and still be classified as an h and χ Per member. The cutoff limits in the second model include the effect of binarity.

[a] Data from S02 and 2MASS.

[b] Data from 2MASS.

the condition set in equation (3). The IR excess population is analyzed through $J = 15$.

As additional checks of the reliability of the data, we examined the individual frames for the sources with apparent excesses and considered as highest weight the excesses detected at *both* [5.8] and [8]. We quantify the excess population at both [5.8] and [8] as well.

5.4. *IR Excess Population: Restrictive Model*

We show the size of the IR excess population relative to the total population as a function of J magnitude for our restricted model (model 1) for $K_s - [4.5]$, $K_s - [5.8]$, and $K_s - [8]$ in Figure 16. The most striking feature in the diagram is the complete lack of IR excess sources at any band for $J \leq 13.5$: 0/250 sources with $J = 11$–13.5 have IR excess. We only begin to detect excess sources at [8] by $J = 13.9$. The IR excess population at [4.5] and [5.8] only starts to appear by $J \sim 14.05$. While our approach may underestimate the fraction of IR excess sources near our faint limit of $J = 14.5$ ($M \sim 1.6\ M_\odot$), sources with $J = 11$–13.5 typically have small photometric errors (≤ 0.05 mag) at all 2MASS and IRAC bands. Thus, we have not missed IR excess sources brighter than $J = 13.5$ ($M \sim 2.7\ M_\odot$) from our sample.

We note two other features in the IR excess population. The [8] IR excess fraction is consistently larger than at [4.5] and [5.8]. This result is consistent with an inside-out clearing of circumstellar disks. Stars with $J = 14$–14.5 (2.2–1.6 $M_\odot$ also tend to have a larger fraction of IR excess sources than stars with $J = 13.5$–14.

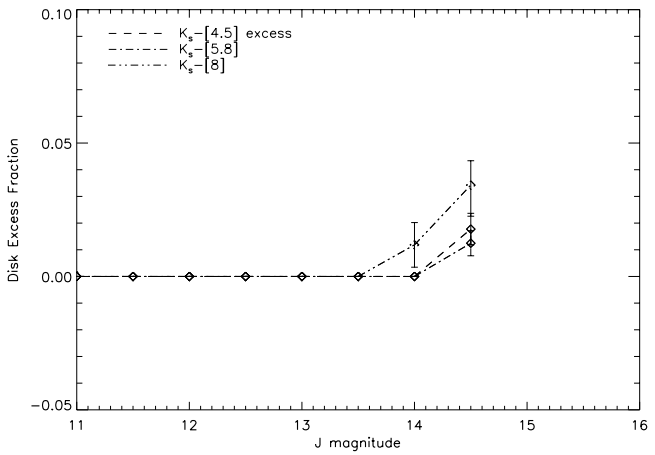

FIG. 16.—Disk fraction at 4.5, 5.8, and 8 μm as a function of J magnitude according to model 1. Fractional excesses are estimated in 0.5 mag bins from 10.5 through 14.5, which corresponds to a range in mass of 7–1.6 $M_\odot$ for $d \sim 2.34$ kpc. The IR-excess population is larger for fainter sources. We detect no excess sources with $J \leq 13.5$. About 3.5% of sources $\sim$1.6 $M_\odot$ have IR excess and may harbor circumstellar disks.

For $J = 14$–14.5, 14/409 ($3.4^{+0.9}_{-1.0}$ %) sources have IR excess at [8]; for $J = 13.5$–14 only 2/169 (1.2% $\pm$ 0.8%) of sources have [8] excess. This result coupled with the lack of excess sources at $J \leq 13.5$ suggests that the frequency of IR excess sources is related to stellar properties.

5.5. *IR Excess Population: Less Restrictive Model*

Now we investigate the IR excess population as a function of J magnitude for our less restrictive model (model 2; Fig. 17). While this approach may introduce more nonmembers, the larger number of cluster members in this sample (to $J \leq 15.5$) yields a larger statistical significance for our results. There are no IR excess sources for $J \leq 13.5$ (0/399) with $J = 11$–13.5 have IR excess at [8] or at shorter wavelengths. Thus, the lack of IR excess sources at IRAC bands to $J = 13.5$ is model independent.

The IR excess population from this sample appears remarkably similar to the restrictive sample where the two overlap (to $J = 14.5$). In both models the [8] excess population is consistently larger than that at [4.5] and [5.8]. The IR excess population at [8] increases from 1.6% $\pm$ 0.6% (8/496) of the total population from $J = 13.5$–14 to $3.5^{+0.6}_{-0.9}$ % (34/983) at $J = 14$–14.5. This result agrees with the estimates (complete to $J = 14.5$) derived in § 5.4. Thus to $J = 14.5$, our estimates of the IR excess population's size is not sensitive to whether we use the long-baseline $V/V-J$ or the short-baseline $J/J-H$ diagram to constrain cluster

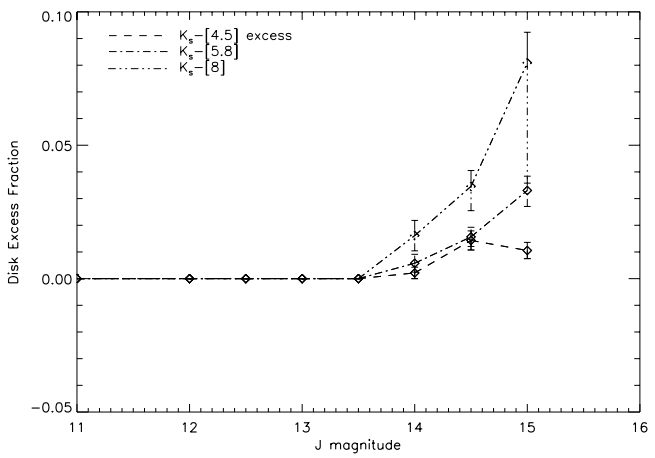

FIG. 17.—Disk fraction at 4.5, 5.8, and 8 μm as a function of J magnitude for model 2. Fractional excesses are estimated in 0.5 mag bins corresponding to a mass range of 7–1.4 $M_\odot$. The results are consistent with those in Fig. 16 (model 1). The IR excess population is clearly larger for fainter sources to $J = 15.0$. There are no IR excess sources for $J \leq 13.5$ ($\sim$2.7 $M_\odot$), which implies that disk lifetimes are larger for lower mass stars (to $\sim$1.4 $M_\odot$). The IR excess population is also consistently larger at progressively longer wavelengths, as expected if the disk lifetime in the hotter, inner disk is shorter than in the cooler, outer disk. About 4%–8% of sources to $J = 15$ have IR excess and may possess circumstellar disks.

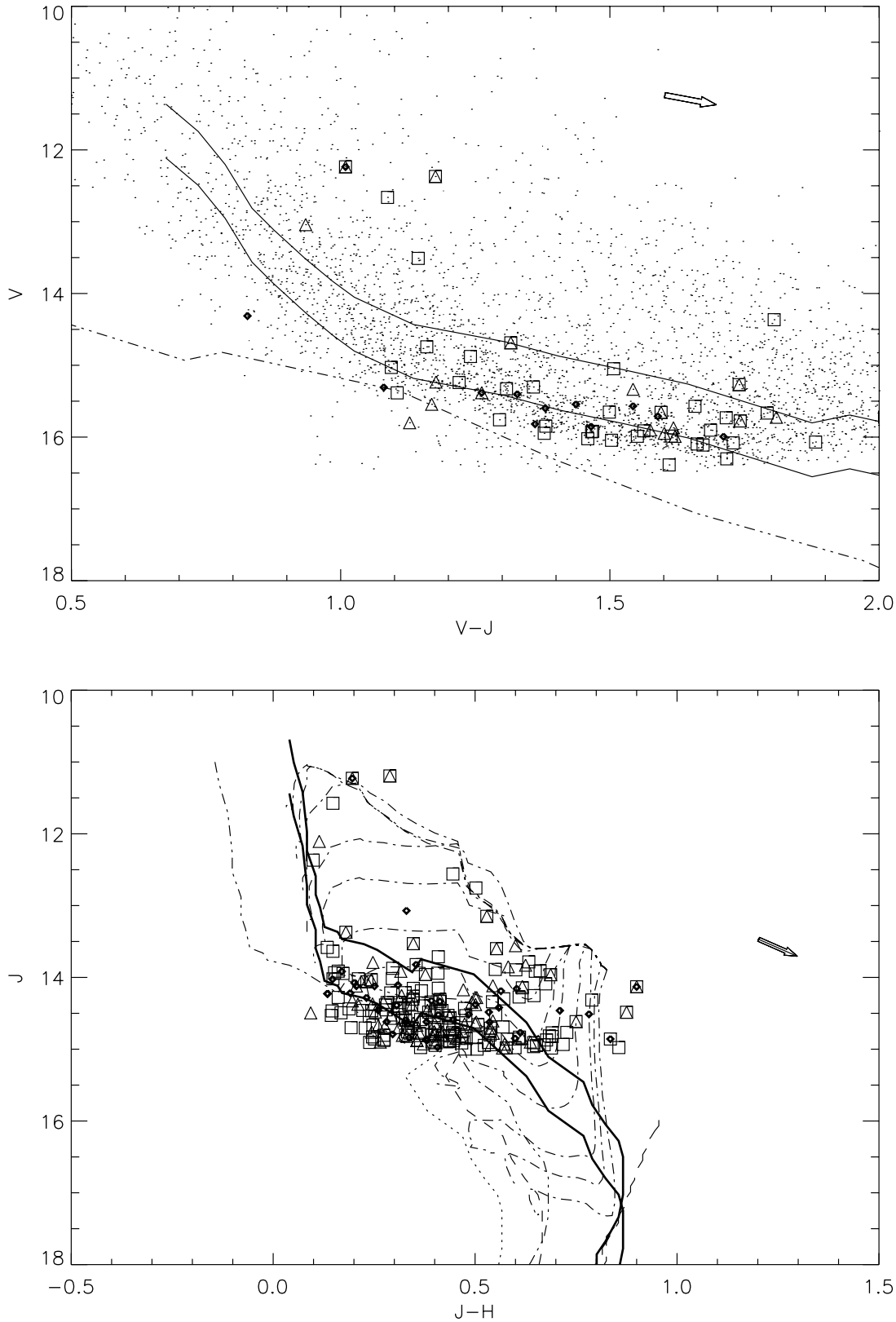

FIG. 18.— Distribution of IR excess sources on CMDs of all sources. Both plots show the $K_s - [4.5]$ (*filled diamonds*), $K_s - [5.8]$ (*triangles*), and $K_s - [8.0]$ (*squares*) excess and $J \leq 15.5$. Arrows correspond to the appropriate reddening vectors as in Fig. 8. In the top panel, the $V/V - J$ distribution for S02 sources with the IR excess sources is overplotted. The reddened 13 Myr isochrone (*dash-two dotted line*), the isochrone for unresolved binaries (*top solid line*) and the unreddened isochrone (*bottom solid line*) are shown, assuming $A_V \sim 3.12E(B - V) \sim 0.16$ and $E(V - J) \sim 1.16$ (Bessel & Brett 1988). The vast majority of IR excess sources are consistent with the 13 Myr isochrone. The bottom panel shows the 2MASS $J/J - H$ diagram of for IR excess sources with. The reddened 13 Myr isochrone (assuming $A_J \sim 0.46$, $E(J - H) \sim 0.185$ extinction) the 13 Myr isochrone for unresolved binaries are shown as the bottom and top solid black lines, respectively. The unreddened 13 Myr isochrone is also shown (*dash-two dotted lines*). Again the vast majority of IR excess sources are consistent with the 13 Myr isochrone and thus are consistent with cluster membership.

membership. For $J = 14.5–15$ the IR excess population at [8] is $\sim 8.1^{+1.1}_{-4.5}$ % (50/618). The population of sources with $J = 14.5–15$, $K_s \leq 14.5$, and [8] detected with errors ≤ 0.2 is smaller than the total population of sources with $J = 14.5–15$ and $K_s \leq 14.5$: this accounts for the relatively large lower bound error. We note that if the sample were restricted to K_s, [8] ≤ 14.25, where completeness is better, the percentage of excess sources is roughly halfway between our measured value of 8.1% and the lower limit of ~4% at ~6.3%. Thus, the IR excess population at [8] near the brightness limit of our analysis comprises about 4%–8% of the total population.

The excess population at $K_s - [4.5]$ is consistently the smallest, ranging from zero through $J = 13.5$ to $0.2\% \pm 0.2\%$, $1.4\% \pm 0.4\%$ (16/1117), to $1.0^{+0.5}_{-0.6}$ % (11/1138) of the total population from $J = 13.5–14$, 14–14.5, and 14.5–15, respectively. Over the same range in J magnitude the [5.8] excess population represents respectively zero, $0.6\% \pm 0.3\%$, $1.6\% \pm 0.4\%$ (19/1214), and $3.3^{+0.5}_{-0.6}$ % (38/1150) of the total population.

5.6. *Sources with Clear IR Excess at Both [5.8] and [8]*

If the IR excess population is dominated by sources with optically thick circumstellar disks extending to the magnetospheric truncation radius (Kenyon et al. 1996), then the IR excess population at [5.8] and [8] should be nearly identical. However, in both models for analyzing the IR excess population, the fraction of sources with IR excess at [8] is consistently larger. It is plausible that sources may not have IR excess at short-wavelength IRAC bands but have excess beyond ~5–10 μm, especially at 10–20 Myr. For example, TW Hya, a 10 Myr T Tauri star, has photospheric colors through [4.5], and a clear IR excess only at [8] (Hartmann et al. 2005). Other evolved T Tauri stars, such as the "transitional" T Tauri stars in Taurus (Kenyon & Hartmann 1995), have SEDs consist with a star+circumstellar disk where the disk has an inner hole. Sources with strong IR excess longward of [5.8] may also be explained by debris produced by planet formation (Kenyon & Bromley 2004; T. Currie et al. 2007, in preparation). However, unlike for TW Hya and similar systems, we do not have constraints beyond 8 μm on IR excess candidates in h and χ Per since the MIPS completeness limit is typically too bright to detect these candidates (T. Currie et al. 2007, in preparation; Z. Balog & T. Currie et al. 2007, in preparation).

Therefore sources with both [5.8] and [8] excess set an absolute lower limit on the size of the IR excess population. We set the excess criteria to $K_s - [5.8,\ 8] \geq 0.4$ and use our sample from model 2. The IR excess population at both [5.8] and [8] begins at $J = 13.8$ and represents ~1% of the population for sources with $J = 14–14.5$. This percentage increases to ~2.2% for $J = 14.5–15$, slightly less than but still consistent with the excess fraction at [5.8] alone from model 2. We also recover the same IR excess population versus J magnitude relation in models 1 and 2, albeit at a lower statistical significance.

Thus, for sources with $M \sim 1.4–1.6\ M_\odot$ at least ~2%–3% have IR excess at both [5.8] and [8]. If we include sources with photospheric colors at all wavelengths short of 8 μm then about ~4%–8% of sources with $J = 14.5–15$ have IR excess.

5.7. *Distribution of IR Excess Sources on $V/V - J$ and $J/J - H$ Color-Magnitude Diagrams*

Here we consider estimates of the IR excess population without cluster membership criteria. If IR excess sources are distributed randomly in $V/V - J$ or $J/J - H$ space our IR excess population estimates might be invalid. Figure 18 shows our results. In the top panel IR excess sources with V-band photometry from S02 preferentially lie along the 13 Myr isochrone. *They are far more clustered around the isochrone than the distribution of all sources*. This trend also prevails for sources without V-band photometry, as shown in the bottom panel of Figure 18. Here the IR excess population is preferentially clustered along the 13 Myr $J/J - H$ isochrone. Just over half of the sources within 25′ of h and χ Per are foreground/background stars, so the sizes of the h and χ Per population and foreground/background populations are comparable. However, the IR excess population for h and χ Per cluster and halo population members is clearly larger than the population of non members. This result is expected if our membership and IR excess criteria are valid.

5.8. *Statistical Trends in the IR Excess Population of h and χ Per*

To conclude, analyzing the excess populations at $K_s - [4.5]$, [5.8], and [8] according to our two models leads to the following trends. First, both models show a complete lack of h and χ Per sources with $J \leq 13.5$ *and* IR excess at any band. This result suggests that *almost all inner disks* ($\leq$ *about 1 AU from the star*) *around massive stars* ($\geq$*2.5–3 $M_\odot$*) *disappear prior to ~10 Myr*. Second, both models show a general increase in the IR excess population with J magnitude. This suggests that *a small number of disks around lower mass stars* (*to ~1.4–1.6 $M_\odot$*) *have lifetimes longer than ~10 Myr*. Third, to $J = 14.5$ (~1.6 $M_\odot$) about 3%–4% of sources have IR excess in the IRAC bands.

The deeper completeness and stronger statistical constraints from model 2 separately yield the following additional results. The IR excess population is larger at [8] than at [5.8] and, especially, [4.5]. This result is consistent with an inside-out clearing of disks. About 4%–8% of sources slightly more massive than the Sun ($J = 14.5–15$, ~1.4–1.6 $M_\odot$) have IR excess. Tighter constraints on the cluster membership from optical spectroscopy and deeper IRAC and MIPS observations will be required to more precisely determine the IR excess population.

6. SUMMARY, FUTURE WORK, AND DISCUSSION

We have conducted the first deep IR survey of the double cluster, h and χ Per. The survey combines 2MASS JHK_s data with deeper JHK_s data from the Lowell Mimir camera and *Spitzer* IRAC 3.6–8 μm data covering a region with an area of roughly 0.75 deg^2. To derive the fraction of stars with IR excesses, we considered the observed stellar surface density distribution, optical and infrared color-magnitude diagrams, and infrared color-color diagrams. This analysis yields the following robust results:

1. For stars with $J \leq 15.5$, the stellar surface density peaks at 15 arcmin^{-2}. In both clusters, the density falls to background levels of ~2.7 arcmin^{-2} ~15′ away from the center peak. About ~47% of the stars within 15′ are cluster members. Comparisons of color-magnitude diagrams show that ~41% of the stars at 15′–25′ from the cluster centers are of approximately the same age, distance, and reddening. In both cases, the Siess et al. (2000) evolutionary tracks suggest ages of ~13 Myr for cluster stars.
2. For stars with $J < 13.5$, the two clusters have essentially no stars with IR excess at $\lambda \lesssim 8$ μm. This result demonstrates that disk emission with $R \lesssim 1$ AU disappears from stars with $M \gtrsim 2.5–3\ M_\odot$ on timescales of $\lesssim$10–15 Myr.
3. Many stars with $J = 13.5–15$ have IR excesses: $\gtrsim$2%–3% of the stars in this magnitude range have excesses at both [5.8] and [8.0]. Combined with the lack of detectable excesses for brighter stars, these results suggest that the disk evolution time depends on the stellar mass, with lower mass stars having longer disk evolution timescales.

In addition to these firm conclusions, our analysis indicates the following more tentative results:

1. If the requirement that sources have excesses at both [5.8] and [8] is relaxed, the fraction of sources with IR excesses increases from 3%–4% at $J = 14$–14.5 to 4%–8% at $J = 14.5$–15.

2. At a fixed brightness, a larger fraction of sources appear to have excesses at longer wavelengths, 5.8–8 μm, than at shorter wavelengths, 4.5 μm. This result is consistent with an inside-out clearing of protoplanetary disks, as proposed in standard theories of planet formation.

These results demonstrate that h and χ Per are an excellent laboratory for studying the evolution of circumstellar disks at 10–15 Myr. With $\geq$5000 sources more massive than the Sun and a potentially significant halo population outside the main cluster boundaries, h and χ Per are at least as populous as the Orion Nebula Cluster (ONC; Hillenbrand 1997) and are the most populous nearby clusters in this age range within 2–3 kpc. Detailed comparisons of these clusters with the ONC and other young clusters provide robust tests of the universality of the IMF (S02) and the evolution of small-scale structures within the clusters (Hillenbrand & Hartmann 1998, BK05).

Further progress on understanding the nature of the IR excess population requires deeper IR imaging surveys and comprehensive spectroscopic surveys. Current near-IR imagers on 4–10 m class telescopes can reach 0.5 $M_\odot$ stars ($J \sim 17.5$) in a few nights. When combined with a deeper IRAC survey ([3.6, 4.5] $\sim$ 16–17, [5.8, 8] $\sim$ 16), these data would yield measures of the IR excess for low-mass stars for which the predicted timescales and outcomes for disk evolution and planet formation are much different than at 1–3 $M_\odot$ (Plavchan et al. 2005; Laughlin et al. 2004). Modern multiobject optical spectrographs routinely acquire high-S/N spectra of $V = 19$–20 stars in 30–45 minutes. With current spectroscopic samples complete only to $V \sim 15$–16 (S02, BK05), a deep spectroscopic survey enables more reliable measures of cluster membership and deep searches for Hα emission for stars with masses of $\sim$0.5–2 $M_\odot$.

We thank Lori Allen, Peter Plavchan, Rudy Schild, Rob Gutermuth, and Nancy Evans for useful comments, Lionel Siess for use of the stellar evolution tracks, and Amanda Bosh for assistance with data acquired during the Mimir observing run. We also thank Charles Lada for initially suggesting *Spitzer* observations of h and χ Persei. Finally, we thank the anonymous referee for a thorough review of the manuscript. T. Currie is supported by an SAO Predoctoral Fellowship. Z. B. received support from Hungarian OTKA Grants TS049872, T042509, and T049082. We acknowledge additional support from the NASA Astrophysics Theory Program grant NAG5-13278 and the Spitzer GO Program (proposal 20132). This work was partially supported by contract 1255094, issued by the Jet Propulsion Laboratory (JPL), California Institute of Technology, to the University of Arizona. This publication makes use of data products from the Two Micron All Sky Survey, which is a joint project of the University of Massachusetts and the Infrared Processing and Analysis Center/California Institute of Technology, funded by the National Aeronautics and Space Administration and the National Science Foundation. This research has made use of the NASA/IPAC Infrared Science Archive, which is operated by JPL, Caltech,, under contract with NASA.

REFERENCES

Alexander, R., et al. 2006, MNRAS, 369, 229
Alibert, Y., et al. 2005, ApJ, 626, L57
Allen, L., et al. 2004, ApJS, 154, 363
Baraffe, I., et al. 1998, A&A, 337, 403
Bernasconi, P. 1996, A&AS, 120, 57
Bertin, E., & Arnouts, S. 1996, A&AS, 117, 393
Bessel, M., & Brett, J. 1988, PASP, 100, 1134
Binney, J., & Tremaine, S. 1987, Galactic Dynamics (Princeton: Princeton Univ. Press)
Borgman, J., & Blaauw, A. 1964, Bull. Astron. Inst. Netherlands, 17, 358
Bragg, A. 2004, Ph.D. thesis, Harvard Univ.
Bragg, A., & Kenyon, S. 2002, AJ, 124, 3289
———. 2005, AJ, 130, 134 (BK05)
Capilla, G., & Fabregat, J. 2002, A&A, 394, 479
Carpenter, J. 2001, AJ, 121, 2851
Carpenter, J., Mamajek, E. E., Hillenbrand, L. A., & Meyer, M. R. 2006, ApJ, 2006, 651, L49
Clarke, C., et al. 2001, MNRAS, 328, 485
Crawford, D., et al. 1970, AJ, 75, 822
Currie, T. 2005, ApJ, 629, 549
Dougherty, S., et al. 1991, AJ, 102, 1753
———. 1994, A&A, 290, 609
Dullemond, C., & Dominik, C. 2005, A&A, 434, 971
Fazio, G. G., et al. 2004, ApJS, 154, 10
Gutermuth, R., et al. 2004, ApJS, 154, 374
Haisch, K., et al. 2001, ApJ, 553, L153
Hartmann, L., et al. 2005, ApJ, 629, 881
Hillenbrand, L. 1997, AJ, 113, 1733
———. 2005, in A Decade of Discovery: Planets Around Other Stars, ed. M. Livio (Baltimore: STScI), preprint (astro-ph/0511083)
Hillenbrand, L., & Hartmann, L. 1998, ApJ, 492, 540
Hillenbrand, L., et al. 1998, AJ, 116, 1816
Keller, S. C., et al. 2001, AJ, 122, 248
Kenyon, S., & Bromley, B. 2004, ApJ, 602, L133
Kenyon, S., & Hartmann, L. 1995, ApJS, 101, 117
Kenyon, S., et al. 1996, ApJ, 462, 439
Laughlin, G., Bodenheimer, P., & Adams, F. C. 2004, ApJ, 612, L73
Mamajek, E., et al. 2004, ApJ, 612, 496
Marco, A., & Bernabeu, G. 2001, A&A, 372, 477
Massey, P. 2003, ARA&A, 41, 15
McCabe, C., et al. 2006, ApJ, 636, 932
Meyer, M. R., Calvet, N., & Hillenbrand, L. A. 1997, AJ, 114, 288
Oosterhoff, P. 1937, Ann. Sternw. Leiden, 17, 1
Plavchan, P., et al. 2005, ApJ, 631, 1161
Quijada, M., et al. 2004, Proc. SPIE, 5487, 244
Reach, W., et al. 2005, PASP, 117, 978
Schild, R. 1967, ApJ, 148, 449
Siess, L., et al. 2000, A&A, 358, 593
Skrutskie, M. F., et al. 2006, AJ, 131, 1163
Slesnick, C., et al. 2002, ApJ, 576, 880 (S02)
Strom, K., et al. 1989, AJ, 97, 1451
Tapia, M., et al. 1984, Rev. Mex. AA, 9, 65
Vogt, N. 1971, A&A, 11, 359
Wildey, R. 1964, ApJS, 8, 439
Youdin, A., & Chiang, E. 2004, ApJ, 601, 1109
Youdin, A., & Shu, F. 2002, ApJ, 580, 494
Young, E., et al. 2004, ApJS, 154, 428